Pascal Heim, BSc

Analysis of molecular Rydberg state relaxation dynamics applying Bayesian probability theory

MASTER'S THESIS

For obtaining the academic degree
Diplom-Ingenieur

Master Programme of
Technical Physics

Graz University of Technology
Institute of Experimental Physics

Supervisor:
Ass.-Prof Dipl.-Ing. Dr. Markus Koch
Institute of Experimental Physics

Graz, April 2017

EIDESSTATTLICHE ERKLÄRUNG

AFFIDAVIT

Ich erkläre an Eides statt, dass ich die vorliegende Arbeit selbstständig verfasst, andere als die angegebenen Quellen/Hilfsmittel nicht benutzt, und die den benutzten Quellen wörtlich und inhaltlich entnommenen Stellen als solche kenntlich gemacht habe. Das in TUGRAZonline hochgeladene Textdokument ist mit der vorliegenden Masterarbeit/Diplomarbeit/Dissertation identisch.

I declare that I have authored this thesis independently, that I have not used other than the declared sources/resources, and that I have explicitly indicated all material which has been quoted either literally or by content from the sources used. The text document uploaded to TUGRAZonline is identical to the present master's thesis/diploma thesis/doctoral dissertation.

_____ _____

Datum / Date Unterschrift / Signature

Abstract

The temporal behaviour of acetone molecules after photo-excitation to high lying Rydberg states was investigated with a pump-probe laser setup for time-resolved femtosecond spectroscopy in combination with the photo-electron photo-ion coincidence (PEPICO) detection method. The approach of an existing collinear setup was changed to non-collinear, which makes it possible to measure with even shorter laser pulses. 800 nm and sub 25 fs laser pulses were frequency doubled to 400 nm in order to excite acetone molecules into high lying Rydberg states with a multi-photon excitation of three photons. With a time delayed and also frequency doubled laser pulse the acetone molecules were ionized with a single photon. Because the three photon excitation is only possible at high pulse intensities the pump pulses created a background spectrum. A method based on Bayesian probability theory was developed to subtract this background signal from the pump-probe spectrum and also obtain an error estimation of this subtracted spectrum. The method is superior over simple subtraction because the result is much smoother, less noisy and no negative signals are possible. The method shows its strength at high time delays where the probe signal is very weak. In order to achieve such an improvement in the signal quality, knowledge of the ionisation and detection process is used.

With this Bayesian subtraction method the time-resolved PEPICO spectra are analysed with a much higher resolution and the complete temporal behaviour of different acetone photo-electronpeaks can be analysed for the first time. With an introduced classical decay model the temporal behaviour of the different acetone peaks can be fitted and the time constants of different states can be determined. A global fit method is used because some states are filled via the decay of the high lying Rydberg states. This means that the population of these states are coupled. The time constants of the different states depend on their energy. Lower lying states have a longer time constant. The time constants of the different states are determined to: $\tau_{3p} = (175 \pm 20)$ fs, $\tau_{3d} = (138 \pm 21)$ fs, $\tau_{4s} = (134 \pm 51)$ fs, $\tau_{4p} = (144 \pm 29)$ fs, $\tau_{Sn1} = (110 \pm 27)$ fs, $\tau_{Sn} = (284 \pm 25)$ fs.

The results will lead two peer-reviewed journal publications: One describing the Bayesian probability subtraction and a second presenting the relaxation dynamics in acetone.

Kurzfassung

Das zeitliche relaxationsverhalten von Aceton nach Photoanregung zu hoch angeregten Rydberg Zuständen wurde mit einem Pump-Probe laser Setup mit Femtosekundenauflösung in Kombination mit der Photoelectron Photoion Coincidence (PEPICO) Methode untersucht. Das kolineare Setup wurde zu einem nicht kolinearen Setup umgebaut um die Zeitauflösung zu erhöhen. 800 nm und sub 25 fs laser Pulse wurden zu 400 nm pulsen frequenzverdoppelt um die Aceton Moleküle mittels Drei-Photon-Anregung in Rydbergzustände anzuregen. Die angeregten Moleküle wurden zeitversetzt mit einem ebenfalls frequenzverdoppelten Photon ionisiert. Da die multiphoton Anregung eine hohe Photonendichte benötigt, erzeugt der Pumppuls ein Hintergrundspektrum. Um diesen Hintergrund aus dem Pump-Probe Spektrum herauszurechnen wurde ein Algorithmus mittels Bayesscher Wahrscheinlichkeitstheorie entwickelt. Mithilfe dieses Algorithmus ist es außerdem möglich eine Unsicherheitsabschätzung des Spektrums zu berechnen. Das mittels Bayes berechnete Spektrum ist glatter und weniger verauscht als ein Spektrum dessen Hintergrund subtrahiert wurde. Die neue Methode zeigt ihre Überlegenheit bei großen Verzögerungszeiten wo wenig Signal im Pump-Probe Spektrum enthalten ist.

Mittels der Bayesschen Subtraktionsmethode konnten die zeitaufgelösten PEPICO Spektren mit sehr hoher Auflösung vermessen werden. Das zeitliche Verhalten verschiedener Zustände konnte so mit einer nie dagewesenen Auflösung bestimmt werden. Die Zeitverläufe wurden mit einem klassischen Zerfallsmodell Zustandsaufgelöst global gefittet. Der globale Fit ist notwendig, da energetisch tiefere Zustände über höhere Rydbergzustände gefüllt werden.
Die Zeitkonstanten von verschiedenen Zuständen sind abhängig von deren Energien. Niederenergetische Zustände zeigen dabei höhere Lebenszeiten. Die ermittelten Zeitkonstanten belaufen sich zu$\tau_{3p} = (175 \pm 20)$fs, $\tau_{3d} = (138 \pm 21)$fs, $\tau_{4s} = (134 \pm 51)$fs, $\tau_{4p} = (114 \pm 29)$fs, $\tau_{Sn1} = (110 \pm 27)$fs, $\tau_{Sn} = (284 \pm 25)$fs.

Die Ergebnisse werden in zwei von Experten geprüften Journalen publiziert: Ein Paper befasst sich mit der Bayesschen Subtraktionsmethode und das andere mit den relaxationsdynamiken in Aceton.

Contents

CHAPTER 1

Introduction

1.1 Pump-Probe Experiments

Dynamics of molecules can be studied by pump-probe experiments. The duration of the pump and the probe pulses have to be at least comparable to or shorter than the time scale of the dynamics. A good analogy is photography. If the exposure time is too long the image is blurred. In pump-probe experiments the same holds true but instead of an image, the population N of a certain state is measured after excitation (with a time delay Δt). In the experiments the acetone molecules are excited with multi-photon excitation and therefore the pump pulses are very intense. Figure 1.1 shows the process schematically. The intense pump pulse excites the molecule in a high lying Rydberg state (green state). The population of this state increases during the pulse. At the same time the population of the state decays via other states back into the ground state. After a time delay Δt the population of the state is probed with the probe pulse. Therefore, the molecule is ionized and photo-electrons are detected. The kinetic energy of the photo-electrons (red line) contain information in which state the molecule was and about the species (parent or fragment). The quantity of the electrons contain information about the population of this state.

1.2 PEPICO

PEPICO is an acronym for *PhotoElectron PhotoIon in COincidence*. This means that the electron and the ion from the same ionisation event are detected. The big advantage is, if for example, a molecule dissociates during excitation, the photo-electron spectra of the fragment, which usually overlap with that of the parent, can be disentangled. If some variables are changed (pulse length, wavelength, chirp, time delay in a pump-probe measurement, $\cdots$) the impact of these changes on the spectra can be analysed for every

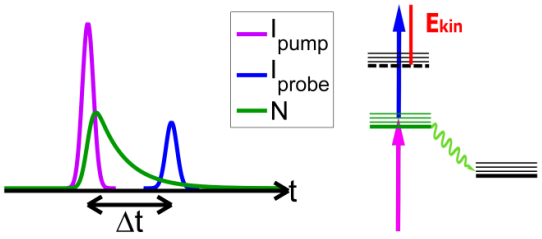

Figure 1.1: Schematics of a pump-probe experiment. A pump pulse excites a certain population N of the molecules into a high lying Rydberg state (green state) which decays over time into other states. After a short time delay Δt the population of the state is probed with the probe pulse which ionizes the molecules (dashed state). The number of detected photo-electrons is proportional to the population of the state. The kinetic energy of the electrons (red line) identifies the state from which the electron originates.

molecule separately (ref. [8]). It is also possible to determine if the molecule dissociated before ionisation or afterwards. If the molecule is ionized and then dissociates the measured photo-electrons of the fragment would have the same energies as that of the unfragmented molecule.
Because the ions and electrons are detected with a certain detection probability it is necessary to work on low count rates to keep false coincidences (detected electron and ion does not originate from the same ionisation event) low. Figure 1.2 shows the dependence of the true to false coincidence ratio. At low ionisation events per laser shot λ the true coincidences dominate because multiple ionisation events are very rare. If the mean ionisation events per laser shot is bigger multiple ionisation events are more common and therefore more false coincidences are detected. At even bigger λ the probability for a coincidence drops because single ionisation events are less probable than multiple ionisation events.

The PEPICO method is used for the acetone measurements because acetone tend to fragment after ionisation if a certain amount of energy (0.79 eV [8], [2]) is converted into vibrational energy. The photo-electron spectra of the acetone parent and acetyl fragment ions overlap. Therefore these two spectra have to be separated. In this thesis the acetone ions are called parent ions and the acetyl ions are called fragment ions.

The measurements in this thesis were performed at a maximum λ of about 0.3 ionisation events per laser shot. This λ corresponds to a true to false coincidence ratio of about 7 ($\xi_e \approx 0.38$, $\xi_i \approx 0.24$ - data from *eiTOF_3360*). Note that this λ is at the overlap where the signal is very strong because of the temporal overlap of the pump and the probe

pulses. However, the relatively low true to false coincidence ratio isnt a problem because the parent and fragment spectra are not compared.

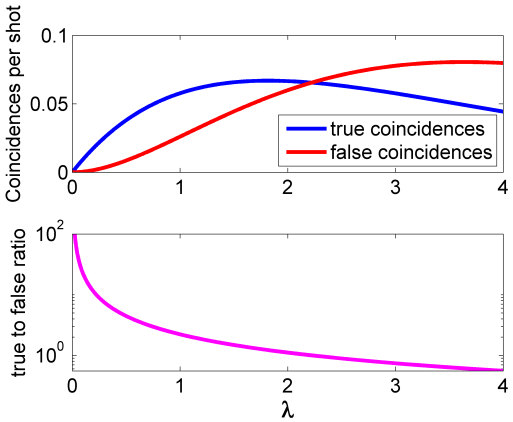

Figure 1.2: Probability to detect a coincidence per laser shot over the mean ionisation events per laser shot λ (detection probability electron: $\xi_e = 0.4$, detection probability ion: $\xi_i = 0.25$). The blue curve represents true coincidences (electron and ion originate from the same ionisation event) and the red line the probability to detect a false coincidence. At few ionisation events per laser shot multiple ionisation events are rare and thus the false coincidences are seldom. This changes if the mean number of ionisation events per laser shot increases. The pink curve shows the ratio of the blue curve with the red one.

1.3 Current Research

Our goal is to investigate different relaxation dynamics (like dissociation, internal conversion, intersystem crossing and vibrational energy redistribution) in acetone. With a pump-probe measurement the dynamical processes can be directly observed [18], [6]. Because of the fact that acetone tend to dissociate the PEPICO technique is necessary to directly observe the dynamics that lead to dissociation [11], [23]. The disadvantage of the PEPICO technique is that it must be performed at low count rates. Therefore, measurements take a long time. If the pump pulses create a background the measurements must be subtracted which takes even longer to get enough statistics. However, the low signal-to-noise ratio cant be avoided if the background is simply subtracted. With Bayesian probability theory the acquired data can be evaluated much more efficiently and therefore increase the signal-to-noise ratio by a lot and also provides an error estimation.

Photoinduced fragmentation of acetone „is one of the most comprehensively investigated

reactions“ [5]. TDDFT calculations show that the highest occupied molecular orbital (HOMO) is described by the electron at the oxigen of acetone which has a non-bonding character [16]. If this electron is excited to a high lying Rydberg state or to the ionic ground state the geometry of the molecule does not change [3]. The Rydberg states decay very efficiently due to internal conversion with crossing valance states [3], [17]. As has recently been shown internal conversion can be very fast [15], [19]. Experiments show that these high lying Rydberg states decay on a femtosecond time scale into lower lying Rydberg states [11], [14]. If more than 0.79 eV are converted into vibrational energy strech the molecule dissociates [8], [2].

CHAPTER 2

Experimental Setup

2.1 Overview

This chapter delivers a short overview of the experimental setup. The different parts are explained in much more detail in the master theses *Ultrafast molecular photodissociation dynamics studied with single-pulse femtosecond photoelectron-photoion-coincidence spectroscopy* by Bernhard Thaler [20] and *Femtosecond Photodissociation Dynamics in Molecules studied by Time-Resolved Photoelectron-Photoion-Coincidence Spectroscopy* by Paul Maierhofer [10]. The part numbers can also be found in Paul Maierhofers thesis. The data acquisition is described in more detail in the master thesis *Multiphoton Ionization Channels in Molecules Investigated by Photoelectron-Photoion-Coincidence Spectroscopy* by Markus Bainschab [1].

The first measurements on this setup were performed by Markus Bainschab and Paul Maierhofer. In their theses they used a collinear setup. The disadvantages of a collinear alignment is that one of the laser pulses has to travel through more matter and is stretched due to dispersion. In this thesis a non-collinear setup is used to avoid this issue.
The experimental setup, which is illustrated in figure 2.1, consist of a commercial Ti:Sapphire laser system (*Vitara* oscillator and a *Legend Elite duo* amplifier from *Coherent Inc.*). It delivers sub 25 fs vertically polarized laser pulses with a central wavelength of 800 nm, a bandwidth of approximately 80 nm and a mean output power of about 13.5 W. The chirp of the laser pulses can be adjusted with a grating compressor which is part of the *Legend Elite duo*. After leaving the *Legend Elite duo* amplifier the pulses are split into two separate paths with a 70/30 beamsplitter (BS). The pulse that is transmitted (more intense) is called pump pulse the other probe pulse. Both paths are basically identical. The only difference is that the pump path has a delay stage where the path length can be adjusted and therefore the time delay between the pump and the probe pulse. Another

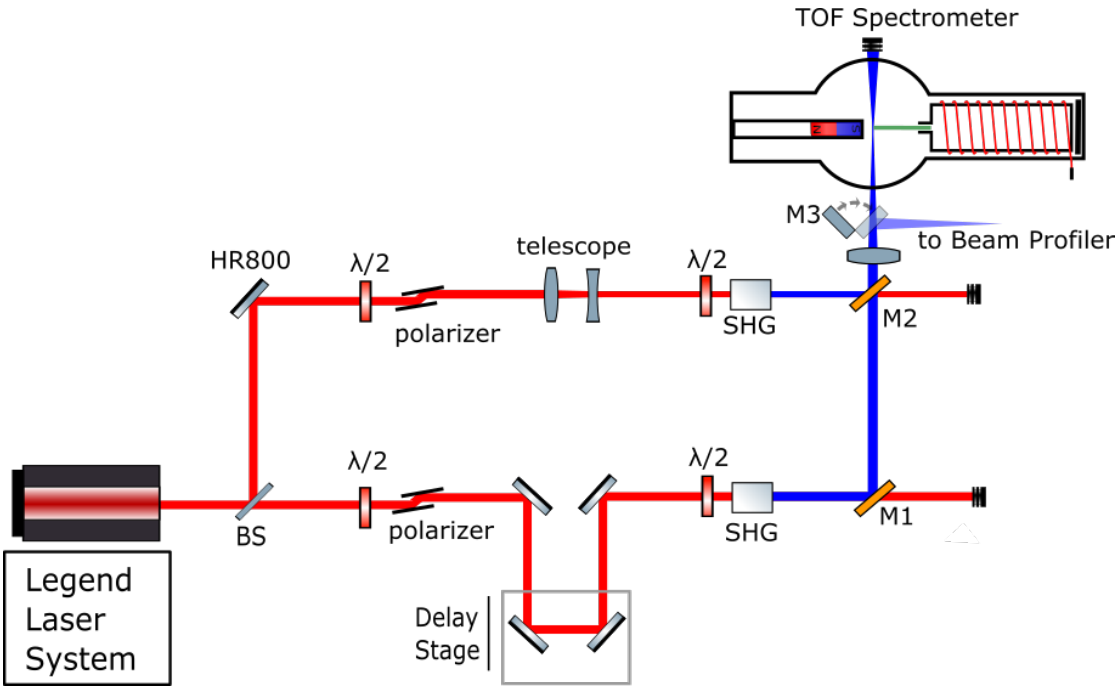

Figure 2.1: Schematics of the experimental setup. Source of the 800 nm laser pulses (full width half maximum < 25 fs) is a commercial *Vitara* oscillator and a *Legend elite duo* amplifier from *Coherent Inc.* The pulses are splitted into two different paths with a 70/30 beam splitter (BS). With the $\lambda/2$ plate and a thin film polariser the intensity of the pulses can be controlled. With another $\lambda/2$ plate and a BBO SHG crystal (thickness: 0.5 mm stage path, 0.2 mm non-stage path) the pulses are frequency doubled. With a HR400/HT800 mirror (M1 and M2) the 800 nm pulses are separated from the 400 nm pulses and focused with a CaF_2 lens into the time of flight spectrometer. There a magnetic bottle setup increases the detection probability of the electrons. One path has a delay stage which allows to control the time delay between the pulses on the two different paths. In the other path is a telescope which is useful to find the spacial overlap of the pulses. Another tool to find the spacial overlap is the Beam Profiler which is a CCD chip. A flipper mirror M3 can redirect the pulses onto the CCD where the two pulses can be seen.

difference is that the probe path has a telescope which changes the diameter of the beam profile. This is useful to increase the conversion efficiency of the second harmonic generation (SHG) process and to find the spacial overlap of the pump and the probe pulse in the time of flight (TOF) spectrometer. The first $\lambda/2$ plate in combination with two

thin film polarisers, which are aligned in Brewster angle, are used to control the intensity of the pulse in the path. The next $\lambda/2$ plate changes the polarization of the 800 nm laser pulse to a horizontal polarization. With the barium borate crystals (BBO - 0.5 mm stage path, 0.2 mm non-stage path) the pulses are frequency doubled. The frequency doubled pulses have a vertical polarisation because the BBO crystals are phase matching type 1 SHG crystals. Then a dichroic mirror which has a high transmittance for 800 nm and a high reflectance for 400 nm light separates the 400 nm from the 800 nm light. The pulses then are focused with a CaF_2 lens with a focus length of 50 cm into the TOF spectrometer. There the acetone molecules (background gas, $p \approx 4.5 \times 10^{-6}$ mbar) are excited and ionized. Then, the electrons are accelerated with a repeller voltage of -3 V towards a chevron Multi Channel Plate (MCP) detector. A magnetic bottle setup [9] allows to accelerate every electron in a 4π sr towards the MCP. Because a single sided PEPICO setup like in ref. [12] is used the repeller voltage has to be switched after a short time delay to +2000 V to also accelerate the ions towards the MCP. The detection of a particle is measurable due to a voltage drop in the MCP phosphor screen voltage. This voltage drop is detected with a *Gage Cobra, Dynamic Signals LLC* card which measures the MCP phosphor screen voltage every half nanosecond. With a *constant value discriminator* the voltage peaks are detected and therefore the flight time of the charged particles.

2.2 Operation Modes

The setup can be used in three different modes:

1. **Electron Mode**
   The repeller voltage is set to -3 V and the coil of the magnetic bottle is used with a current of 3 A. Thereby only electrons are detected.

2. **Ion Mode**
   The repeller voltage is set to +2000 V and the magnetic bottle is turned off. In this configuration only ions are detected.

3. **PEPICO Mode**
   This mode is a mixture of the modes described above. The +2000 V and -3 V repeller voltages are attached to the inputs of a high voltage switch. The output of this switch is connected to the repeller. The magnetic bottle is used at 3 A as in the Electron Mode. This allows to measure the electrons and the ions of the same ionisation event.

For more technical details see the master thesis of Markus Bainschab [1].

2.3 Pump-Probe Overlap

Paul Maierhofer used in his thesis a collinear setup of the pump and the probe beams. The disadvantage of a collinear setup is that the pump pulse passes through more material with the consequence of a changed chirp, but with the advantage that the spacial overlap of the pump and the probe pulse is easier to find because spacial overlap is given at any moment. In this thesis a non-collinear setup is used to avoid the mentioned disadvantages.

2.3.1 Find the Overlap in a Non-Collinear Setup

For the experiments in this thesis a non-collinear setup is used which means that the pulses of the path with the delay stage does not propagate through M2. The advantage is that the pulses propagate through less material and therefore the pulses can be shorter. The spacial overlap is more difficult to achieve in a non-collinear setup and therefore, it is described here in more detail:

1. Measure the power of the 400 nm pump pulse and adjust the grating compressor such that the conversion efficiency is maximized.

2. Find the repeller position where the electron signal of the pump pulses are maximized. The electron signal depends more on the repeller position than the ion signal[1] - finding this signal maximum is easier.

3. Flipper mirror M3 (fig. 2.1) directs the pulses to a CCD chip (when inserting the mirror block out the laser!). Protect the chip with a white card because if the laser pulse hits the CCD directly it will be damaged. Move the pump pulse with the mirror M3 and the probe pulse with M2 across the chip.

4. Insert an ODE-2 and ODE-3 filter to debilitate the intensity. Then additively turn back the intensity with the first $\lambda/2$ plate. Remove the white card.

5. Open the Matlab program *Copy_ of_ profile_ horver.m* to see the CCD signal on the computer screen.

6. Slowly increase the intensity with the $\lambda/2$ plates which are in front of the thin film polariser, that the pulses become visible on the computer screen (figure 2.2). If the background signal on the CCD is too big turn off the light in the laboratory.

7. Block out the probe pulses and position the CCD chip in the focus of the pump pulses. In the focus the diameter of the pulse is minimal. Note that the probe pulses and the pump pulses does not have the same focal width because of spherical aberration.

[1] Markus Bainschab [1] - page 42

8. Adjust mirror M2 such that the pump and the probe pulses are at the same spot on the CCD (fig. 2.2). For a better contrast frequently block out the larger beam.

9. Turn down the pulse intensities and remove the flipper mirror M3 and the ODE filters → the pulses are focused into the spectrometer. Block out the laser while flipping the mirror!

10. Set the intensity with the $\lambda/2$ plates to a value that the pump pulse give about 150 ion counts per second and the probe pulses about 20 ion counts per second. To detect the ions the following steps are necessary (before increasing the intensity):
    - Check chamber pressure: $p \approx 4.5 \times 10^{-6}$ mbar
    - Turn on the MCP voltages (MCP back: 2500 V, MCP front: 2100 V - Voltage difference between MCP back and the phosphor screen should not be bigger than 500 V because of risk of sparks that can damage the MCP)
    - Connect the datacable and the triggercable to the counter.
    - Turn on the +2000 V repeller voltage and connect it to the repeller
    - Make sure that the PC has a connection to the counter

11. Open the Matlab program *timescan_counts_2gates_v2.m* and scan the whole timedelay region. Typical values in the Matlab program are (to find the overlap):
    - stepsize = 0.005 mm → 33 fs
    - intTime = 0.5 s
    - Typical position of the overlap is around 27.4 mm.

12. If no overlap is found (no significant signal increase like in figure 2.3) focus the probe pulses on the CCD (described in steps 3 - 6) and increase the diameter by adjusting the telescope. Do not make the diameter too big - the probe pulses should be able to give a signal by themselves (about 20 ion counts per second).

Figure 2.3 shows an of an example overlap that was found in the time scan. The parent and fragment signal show a clear signal increase at a certain stage position x (green shaded). Also a second overlap can be seen at a very high time delay.
Figure 2.4 shows the overlap in more detail and after optimization. A total signal increase of a factor of 16 in the parent signal was possible. Typical signal increase factors of about 7 are normal.

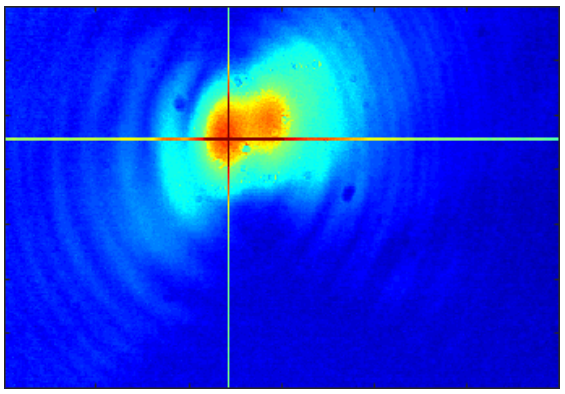

Figure 2.2: Example of the pump and the probe pulse if they are not spatially overlapped. Adjust the probe mirror M2 that both pulses are on the same spot. The dark blue spots are damaged areas on the CCD chip.

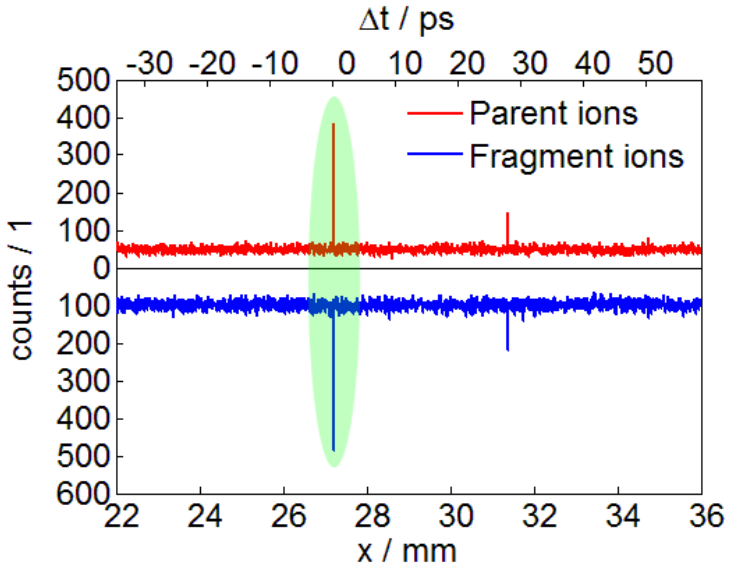

Figure 2.3: Example of an overlap signal (measured 16.08.2016, File: *Timescan-Counts_ 0402*).
The stage scanned from 22 mm up to 36 mm with an integration time of 0.5 s. At the overlap a big signal increase can be seen. Also a second smaller overlap, which is created due to a reflection can be observed.

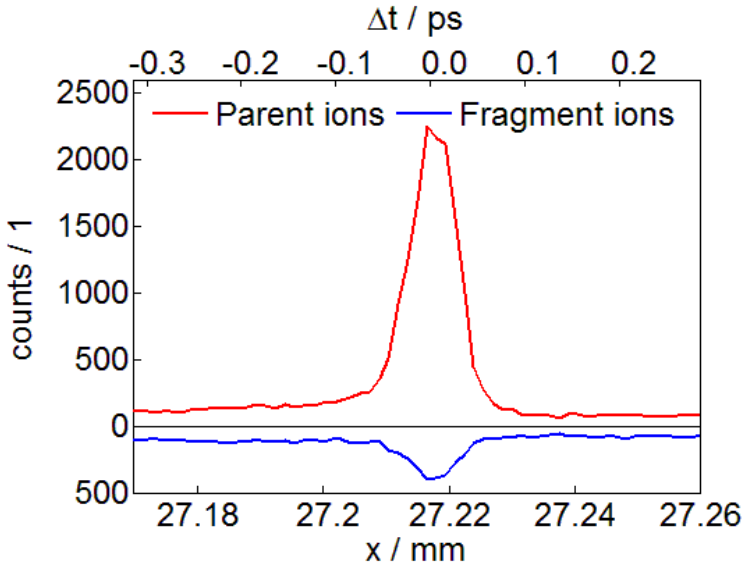

Figure 2.4: A closer look at an optimized overlap signal (measured 16.08.2016, File: *TimescanCounts_0405*).
The signal increase is in the parent signal about the factor 16 which is very good. A normal overlap has a signal increase factor of about 7. The overlap is very narrow and therefore hard to find.

2.3.2 Multiple Pump-Probe Overlaps

It is possible that multiple overlaps are found (figure 2.5). In both pump and probe beams 400 nm and 800 nm pulses are present. The different overlaps represent combinations of 400 nm and 800 nm pulses from the pump and the probe beams. To check which overlap corresponds to which combination of wavelengths the SHG conversion efficiency of the pump/probe pulse was changed by tilting the corresponding SHG crystal and check the signal height of the overlaps. If the conversion efficiency in one path is decreased and the overlap signal height stays constant or raises then the signal originates from a 800 nm pulse from the path where the conversion efficiency was decreased and a 400 nm pulse from the other path. If the signal decreases the 400 nm pulse of this path is responsible for the overlap. Note that there is no 800/800 nm overlap signal because the power of the 800 nm pulses is too low.

In table 2.1 the combination of wavelengths of the pump and the probe pulses are listed which create the different overlaps in figure 2.5. Also the time delays are listed. With the help of figure 2.6 the interpretation of the overlaps is much easier. The two overlaps next to the 400/400 overlap (overlap 2 and 4) are symmetric. They are created with a 800 nm pulse which is ahead of the 400 nm pulse due to dispersion in the lens and the TOF window. The overlap 1 and 5 are due to a reflection. The asymmetry of the time delays show that the reflected pulses of the pump and the probe pulses have taken different optical paths.

Table 2.1: Overview over the different overlaps (which wavelength are responsible for the overlap and at which time delays do they occur). Numbers correspond to figure 2.6.

#	pump wavelength / nm	probe wavelength / nm	path difference / mm	time delay / ps
1	400	800	5.94	-39.60
2	800	400	0.17	-1.13
3	400	400	0	0
4	400	800	-0.16	1.07
5	800	400	-3.99	26.60

The multiple overlaps are a problem because the temporal behaviour of the high lying acetone states should be investigated up to a time delay of about 1.2 ps which is not possible because the nearest additional overlap is at about 1 ps (see tab. 2.1). Only the overlap at a time delay of about 1 ps must be removed because this is the region which will be investigated. To remove this overlap different approaches were tried:

1. Reduce focus size of the non-stage pulses. The overlap on the negative time delay

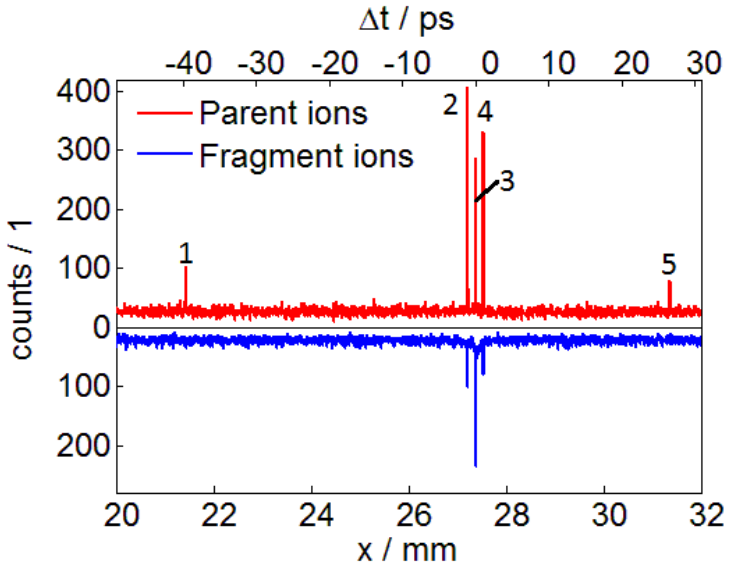

Figure 2.5: Overview of the multiple overlaps (measured 23.08.2016, File: *Timescan-Counts_ 0416*)
Five different overlaps were detected. Overlap 3 is the desired one (400 nm with 400 nm). Overlaps 2 and 4 are symmetric around overlap 3 and are created by 400 nm and 800 nm pulses. They are due to dispersion in the lens and the TOF window. Overlaps 1 and 5 are due to a reflection of the 800 nm pulses. The different reflections had different pathways and therefore are not symmetric. There are no 800/800 nm or a reflective 400/400 nm overlap overlaps because the pulse intensities are too low.

side is reduced.
→ moderate success

2. Increase the SHG conversion efficiency. One of the overlaps is drastically reduced (on the positive time delay side) and the other one is moderately reduced.
→ good success on one side

3. Change pulse path by tilting different mirrors.
→ no success

4. Switch the BBO crystals (from 0.5 mm BBO in the pump (stage) path and 0.2 mm BBO in the probe path (non-stage) to 0.2 mm BBO in the pump path (stage) and 0.5 mm BBO in the probe path (non-stage))
→ no success

With the steps mentioned above only the overlap on the right side was removed. It was not possible to get rid of the other overlap. In order to make measurements the stage path is used for probing and the non-stage path for pumping which can be seen in figure 2.7.

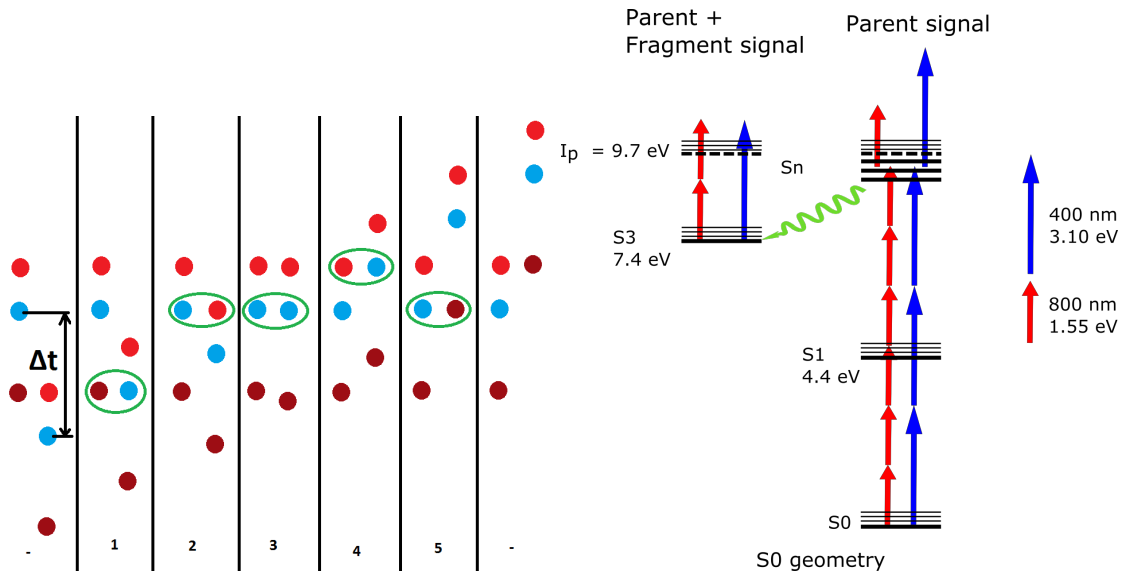

(a) Different pulses in space. Left dots represent the pulses of the non-stage path. Right dots represent the pulses of the stage path. The red dots are 800 nm pulses (dark red dots are due to a reflection) and the blue dots 400 nm pulses.

(b) Term schematic of different ionisation channels. To populate the S_n state 3 400 nm photons are needed or 6 800 nm photons. To probe the S_n channel 1 photon is needed (with 400 and 800 nm). To probe the S_3 state one 400 nm photon or 2 800 nm photons are required.

Figure 2.6: Overview of the origin of the 5 different overlaps.
o 800 nm pulse
o 400 nm pulse
o Detected signal (due to overlap)
The 800/800 nm overlap creates no photo-electron/ion signal because the intensity of the 800 nm pulses is too weak to excite the molecule with a 6 photon excitation. Therefore, every overlap is pumped with 400 nm photons. Overlap 1 and 5 is probed with 800 nm pulses which originates due to a reflection (dark red dots) - the intensity of this 800 nm pulses are low and therefore the two photon excitation to ionize the S_3 state is not possible. Therefore, no fragment ions are detected. The overlap with 800 nm which is ahead of the 400 nm due to dispersion (light red dots) is intense enough to ionize the S_3 state and therefore creates fragment and parent ions.

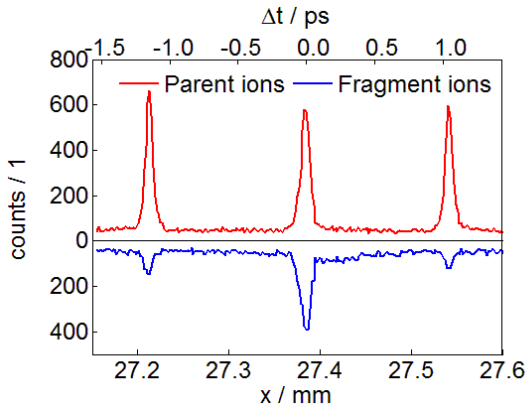

(a) Multiple overlaps before optimizing. Pump-probe side is on the right side. (Pump: stage path)
File: *TimescanCounts_0418* - recorded 23.08.2016

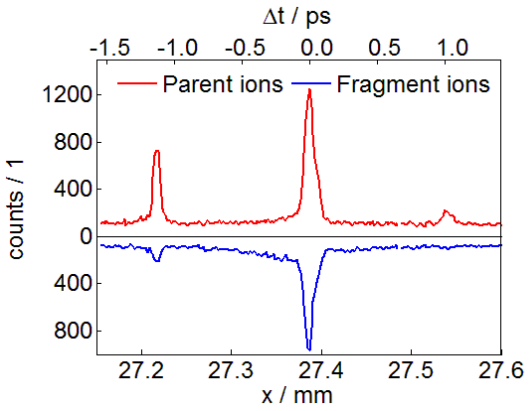

(b) By changing the non-stage focus size and maximizing the conversion efficiency the additional overlaps are reduced (the right one more than the left).
File: *TimescanCounts_0419* - recorded 23.08.2016

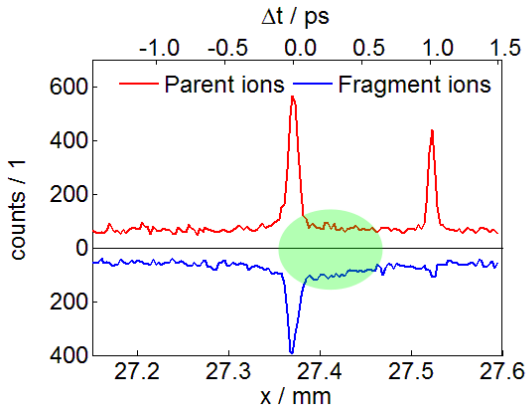

(c) After maximizing the conversion efficiency the left overlap is gone but the right one could not be eliminated. The pump probe side is the right side (dynamics are green shaded).
File: *TimescanCounts_0424* - recorded 24.08.2016

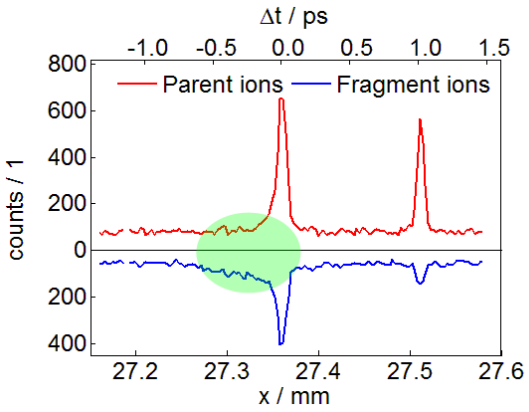

(d) The paths switch their role: The non-stage path pumps the molecule (green shaded dynamics switched sides).
File: *TimescanCounts_0430* - recorded 24.08.2016

Figure 2.7: Figures (a)-(d) show the different stages of getting rid of the additional overlaps. The overlap on the left side is removed by changing the focus size of the non-stage pulses and maximizing the conversion efficiency. It was not possible to remove the right overlap. Afterwards the non-stage path is used for pumping.
BBO crystals in the paths:
Stage path: 0.5 mm
Non-stage path: 0.2 mm

CHAPTER 3

Spectra Subtraction and Basis Transformation

This chapter is the result of a collaboration between the Institute of Experimental Physics TU-Graz (Pascal Heim) and the Institute of Theoretical Physics TU-Graz (Univ.Prof. Dr. Wolfgang von der Linden and Michael Rumetshofer).

3.1 Introduction

3.1.1 The Problem

To excite the acetone molecules to a high lying Rydberg state three 400 nm photons must be absorbed at the same time. This is only possible if the photon density is very high. With such a high photon density another photon can be absorbed and ionize the molecule. Therefore, the pump pulse itself creates ionization events and therefore coincidence counts (background signal). To account for the background it was simply subtracted from the pump-probe spectrum which is quite problematic because the ionization and detection of the ions and electrons are probabilistic events. The results were very noisy spectra at high time delays which also contained negative counts and it was difficult to interpret these spectra. In this chapter a method based on Bayesian probability theory is introduced which uses more information of the measured spectra and not only the function value.

3.1.2 Bayes' Theorem

The probability that A *and* B are true can be written as the probability that A is true if B is already true times the probability that B is true:

$$P(A \wedge B) = P(A|B)P(B) \tag{3.1}$$

The probability that B *and* A is true therefore is:

$$P(B \wedge A) = P(B|A)P(A) \tag{3.2}$$

Note that (3.1) and (3.2) are the same:

$$P(A \wedge B) = P(B \wedge A) \tag{3.3}$$

This leads to Bayes' theorem:

BAYES' THEOREM

$$P(A|B) = \frac{P(B|A)P(A)}{P(B)} \tag{3.4}$$

$P(A|B) \cdots$ Posterior
$P(B|A) \cdots$ Likelihood
$P(A) \cdots$ Prior
$P(B) \cdots$ Evidence

The evidence is usually the probability to measure the measured data and in most calculations this probability is constant. Only in rare cases the evidence must be calculated (for example when data is fitted with a fit function where the probability to measure the data depends on the fit model).

3.1.3 Law of Total Probability (Marginalisation Rule)

If the probability $P(A)$ is not known it is often useful to insert conditions because then the distribution is known. In the following it will be shown how to write $P(A)$ with some conditions $P(A|B_1)$ and $P(A|B_2)$.

The probability that B_1 *or* B_2 is true is the sum of the probabilities that one of them is true. But the probability that B_1 *and* B_2 are true is counted twice in that case. So this probability has to be subtracted once (see figure 3.1)

$$P(B_1 \vee B_2) = P(B_1) + P(B_2) - P(B_1 \wedge B_2) \tag{3.5}$$

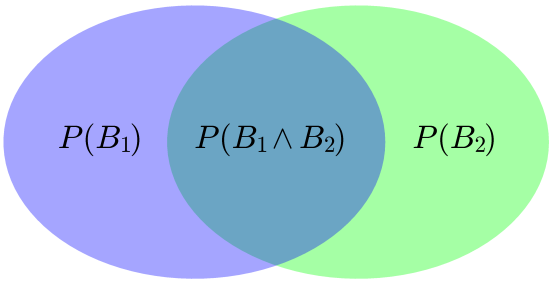

Figure 3.1: The probability $P(B_1 \vee B_2)$ is the whole coloured area: The sum of both ellipses minus the intersection area $(P(B_1) + P(B_2) - P(B_1 \wedge B_2))$ because this area is contained in the green *and* the blue ellipse.

If it is certain that B_1 *or* B_2 is true $(P(B_1 \vee B_2) = 1)$ and it is impossible that B_1 *and* B_2 are true $(P(B_1 \wedge B_2) = 0)$ then $P(A)$ can be rewritten as follow:

$$\begin{aligned} P(A) = P(A \wedge 1) &= P(A \wedge (B_1 \vee B_2)) = P((A \wedge B_1) \vee (A \wedge B_2)) \\ &= P(A \wedge B_1) + P(A \wedge B_2) \\ &= P(A|B_1)P(B_1) + P(A|B_2)P(B_2) \end{aligned}$$

This idea can be generalized:

LAW OF TOTAL PROBABILITY

$$P(A) = \sum_{i=1}^{N} P(A|B_i)P(B_i) \tag{3.6}$$

with the conditions

$$\sum_{i=1}^{N} P(B_i) = 1 \tag{3.7}$$

$$P(B_i \wedge B_j) = 0 \qquad i \neq j \tag{3.8}$$

For much more information about Bayesian probability theory and the law of total probability see [22].

3.2 Coincidence Probability for a Single Source

If light with enough intensity hits a molecule it has a certain probability to ionize it. If there are a lot of molecules the probability to ionize n molecules in a certain time interval is described by a Poisson distribution:

$$p(n|\lambda) = \frac{\lambda^n}{n!} e^{-\lambda} \tag{3.9}$$

With the average number of ionisation events per time interval λ.
A detector for charged particles usually has a detection probability $\xi < 1$. The probability that a detector detects k particles out of n is described by a binomial distribution:

$$p(k|n,\xi) = \binom{n}{k} \xi^k (1-\xi)^{n-k} \tag{3.10}$$

The probability to detect k_e electrons and k_i ions if the average number of ionization events λ and the detection probabilities ξ_e and ξ_i are known is:

$$p(k_e, k_i|\lambda, \xi_e, \xi_i) = \sum_{n=max(k_e,k_i)}^{\infty} p(k_e|\xi_e, n)p(k_i|\xi_i, n)p(n|\lambda)$$
$$= \sum_{n=max(k_e,k_i)}^{\infty} \binom{n}{k_e} \xi_e^{k_e}(1-\xi_e)^{n-k_e} \binom{n}{k_i} \xi_i^{k_i}(1-\xi_i)^{n-k_i} \frac{\lambda^n}{n!} e^{-\lambda} \quad (3.11)$$

The sum starts with $max(k_e, k_i)$ because if k_e electrons are detected then there happened at least k_e ionization events. The same holds true if k_i ions are detected.

To evaluate (3.11) use the abbreviations $k_\downarrow = min(k_e, k_i)$ and $k_\uparrow = max(k_e, k_i)$. If for example $k_e < k_i$ then $\xi_\downarrow = \xi_e$ and $\xi_\uparrow = \xi_i$. If not it is vice versa.

$$p(k_e, k_i|\lambda, \xi_e, \xi_i) = \xi_\downarrow^{k_\downarrow} \xi_\uparrow^{k_\uparrow} e^{-\lambda} \sum_{n=k_\uparrow}^{\infty} \frac{n!(1-\xi_\downarrow)^{n-k_\downarrow}(1-\xi_\uparrow)^{n-k_\uparrow}\lambda^n}{(n-k_\downarrow)!(n-k_\uparrow)!}$$
$$= \xi_\downarrow^{k_\downarrow} \xi_\uparrow^{k_\uparrow} e^{-\lambda}(1-\xi_\downarrow)^{k_\uparrow - k_\downarrow} \underbrace{\sum_{n=k_\uparrow}^{\infty} \frac{n!}{(n-k_\downarrow)!} \frac{[(1-\xi_\downarrow)(1-\xi_\uparrow)]^{n-k_\uparrow}\lambda^n}{(n-k_\uparrow)!}}_{=S}$$

Take a closer look at the sum S:

$$
\begin{aligned}
S &= \sum_{n=k_\uparrow}^{\infty} \overbrace{\frac{n!\lambda^n}{(n-k_\downarrow)!}}^{=\lambda^{k_\downarrow}\frac{\delta^{k_\downarrow}}{\delta\lambda^{k_\downarrow}}\lambda^n} \frac{[(1-\xi_\downarrow)(1-\xi_\uparrow)]^{n-k_\uparrow}}{(n-k_\uparrow)!} \\
&= \lambda^{k_\downarrow}\frac{\delta^{k_\downarrow}}{\delta\lambda^{k_\downarrow}} \sum_{n=k_\uparrow}^{\infty} \frac{[(1-\xi_\downarrow)(1-\xi_\uparrow)]^{n-k_\uparrow}\lambda^n}{(n-k_\uparrow)!} \\
&= \lambda^{k_\downarrow}\frac{\delta^{k_\downarrow}}{\delta\lambda^{k_\downarrow}} \left(\lambda^{k_\uparrow} \underbrace{\sum_{n=k_\uparrow}^{\infty} \frac{[(1-\xi_\downarrow)(1-\xi_\uparrow)\lambda]^{n-k_\uparrow}}{(n-k_\uparrow)!}}_{e^{(1-\xi_\downarrow)(1-\xi_\uparrow)\lambda}} \right) \\
&= \lambda^{k_\downarrow} \sum_{m=0}^{k_\downarrow} \binom{k_\downarrow}{m} \left(\frac{\delta^m}{\delta\lambda^m}\lambda^{k_\uparrow}\right) \left(\frac{\delta^{k_\downarrow-m}}{\delta\lambda^{k_\downarrow-m}} e^{(1-\xi_\downarrow)(1-\xi_\uparrow)\lambda}\right) \\
&= \lambda^{k_\downarrow} \sum_{m=0}^{k_\downarrow} \binom{k_\downarrow}{m} \frac{k_\uparrow!}{(k_\uparrow-m)!} \lambda^{k_\uparrow-m}[(1-\xi_\downarrow)(1-\xi_\uparrow)]^{k_\downarrow-m} e^{(1-\xi_\downarrow)(1-\xi_\uparrow)\lambda}
\end{aligned}
$$

The result is:

PROBABILITY TO DETECT k_e ELECTRONS AND k_i IONS:

$$
\begin{aligned}
p(k_\downarrow, k_\uparrow|\lambda, \xi_\downarrow, \xi_\uparrow) = \xi_\downarrow^{k_\downarrow}\xi_\uparrow^{k_\uparrow}\lambda^{k_\uparrow}(1-\xi_\downarrow)^{k_\uparrow-k_\downarrow} e^{-\lambda(1-(1-\xi_\downarrow)(1-\xi_\uparrow))} \\
\sum_{m=0}^{k_\downarrow} \binom{k_\downarrow}{m} \frac{k_\uparrow!}{(k_\uparrow-m)!} [\lambda(1-\xi_\downarrow)(1-\xi_\uparrow)]^{k_\downarrow-m}
\end{aligned} \tag{3.12}
$$

$$k_\uparrow = max(k_e, k_i) \rightarrow \xi_\uparrow$$

$$k_\downarrow = min(k_e, k_i) \rightarrow \xi_\downarrow$$

IMPORTANT PROBABILITIES $p(k_e, k_i|\lambda, \xi_e, \xi_i)$

$$p(0,0|\lambda,\xi_e,\xi_i) = e^{-\lambda(1-(1-\xi_e)(1-\xi_i))} \tag{3.13}$$

$$p(1,0|\lambda,\xi_e,\xi_i) = \lambda\xi_e(1-\xi_i)e^{-\lambda(1-(1-\xi_e)(1-\xi_i))} \tag{3.14}$$

$$p(0,1|\lambda,\xi_e,\xi_i) = \lambda(1-\xi_e)\xi_i e^{-\lambda(1-(1-\xi_e)(1-\xi_i))} \tag{3.15}$$

$$p(1,1|\lambda,\xi_e,\xi_i) = \lambda\xi_e\xi_i(1+\lambda(1-\xi_e)(1-\xi_i))e^{-\lambda(1-(1-\xi_e)(1-\xi_i))} \tag{3.16}$$

3.3 Coincidence Probability for Two Ion Sources

If there are two source channels of ions λ_1 (for example pump pulse or parent ions) and λ_2 (for example probe pulse or fragment ions) there are more possibilities to detect a coincidence. To calculate the probability for a coincidence the law of total probability is used: marginalize k_e^j and k_i^j into the probability $p(k_e, k_i|\lambda_1, \lambda_2, \xi_e, \xi_i)$. j represents if the charged particle belongs to channel 1 or 2.

$$\begin{aligned} p(1,1|\lambda_1,\lambda_2,\xi_e,\xi_i) &= \sum_{\substack{k_e^1,k_i^1\\k_e^2,k_i^2}} p(k_e^1,k_i^1|\lambda_1,\xi_e,\xi_i)p(k_e^2,k_i^2|\lambda_2,\xi_e,\xi_i)\delta(k_e^1+k_e^2=1)\delta(k_i^1+k_i^2=1) \\ &= \overbrace{p(1,1|\lambda_1,\xi_e,\xi_i)p(0,0|\lambda_2,\xi_e,\xi_i)}^{ZP_1} + \overbrace{p(0,0|\lambda_1,\xi_e,\xi_i)p(1,1|\lambda_2,\xi_e,\xi_i)}^{ZP_2} \\ &+ p(1,0|\lambda_1,\xi_e,\xi_i)p(0,1|\lambda_2,\xi_e,\xi_i) + p(0,1|\lambda_1,\xi_e,\xi_i)p(1,0|\lambda_2,\xi_e,\xi_i) \end{aligned} \tag{3.17}$$

A detected coincidence can originate from four different combinations of electrons and ions. It can be a coincidence from the first or second channel or it can be a mixed coincidence where the electron originates from channel 1 and the ion from channel 2 or vice versa.
The probabilities in (3.17) are already calculated (see (3.13) - (3.16)). P_1 and P_2 are the probabilities that a coincidence in the spectrum originates from channel 1 or channel 2.

This will be useful later.

In the spectrum all counts are one to one coincidences. This means that:

$$\frac{1}{Z}p(1,1|\lambda_1,\lambda_2,\xi_e,\xi_i) = 1 \tag{3.18}$$

$$Z = \xi_e\xi_i\lambda(1+\lambda(1-\xi_e)(1-\xi_i))e^{-\lambda(1-(1-\xi_e)(1-\xi_i))} \tag{3.19}$$

$$\lambda = \lambda_1 + \lambda_2 \tag{3.20}$$

3.3.1 True to False Coincidence Ratio in a Single Pulse Experiment

In a single pulse experiment the channels 1 and 2 are parent or fragment ions. Therefore, it is possible to calculate a true to false coincidence ratio. A true coincidence is a coincidence where the electron and the ion originate from the same channel (for example the parent ion). The total mean ionisation events per laser shot is $\lambda = \lambda_1 + \lambda_2$. The probability for a true coincidence which originates from the same channel (SC) is the probability for a coincidence minus the probability for a false coincidence:

$$\begin{aligned} tf_{SC} = \frac{p_{true}}{p_{false}} &= \frac{p(1,1|\lambda,\xi_e,\xi_i) - 2\lambda_1\lambda_2\xi_e\xi_i(1-\xi_e)(1-\xi_i)}{2\lambda_1\lambda_2\xi_e\xi_i(1-\xi_e)(1-\xi_i)} \\ &= \frac{\lambda+\lambda^2(1-\xi_e)(1-\xi_i)}{2\lambda_1\lambda_2(1-\xi_e)(1-\xi_i)} - 1 \\ &= 1 + \frac{(\lambda_1+\lambda_2)+(\lambda_1-\lambda_2)^2(1-\xi_e)(1-\xi_i)}{2\lambda_1\lambda_2(1-\xi_e)(1-\xi_i)} \end{aligned}$$

Note that this true to false coincidence ratio is always greater than one.

The true to false coincidence ratio for every channel can be calculated independently:

$$tf^i_{SC} = \frac{p(1,1|\lambda_i,\xi_e,\xi_i)p(0,0|\lambda_j,\xi_e,\xi_i)}{2\lambda_1\lambda_2\xi_e\xi_i(1-\xi_e)(1-\xi_i)} = \frac{\lambda_i+\lambda_i^2(1-\xi_e)(1-\xi_i)}{2\lambda_1\lambda_2(1-\xi_e)(1-\xi_i)} \tag{3.21}$$

Markus Bainschab [1] calculated the true to false coincidence ratio with the condition that the detected ion and electron originate from the same ionisation event (see (3.24)):

TRUE TO FALSE RATIO (SAME CHANNEL)

Total:

$$tf_{SC} = 1 + \frac{\lambda_1 + \lambda_2 + (\lambda_1 - \lambda_2)^2(1-\xi_e)(1-\xi_i)}{2\lambda_1\lambda_2(1-\xi_e)(1-\xi_i)} \tag{3.22}$$

Channel resolved:

$$tf^i_{SC} = \frac{\lambda_i + \lambda_i^2(1-\xi_e)(1-\xi_i)}{2\lambda_1\lambda_2(1-\xi_e)(1-\xi_i)} \tag{3.23}$$

TRUE TO FALSE RATIO (SAME IONISATION EVENT)

$$tf_{SI} = \frac{1}{\lambda(1-\xi_e)(1-\xi_i)} \tag{3.24}$$

In the special case of $\lambda_1 = \lambda_2 = \lambda$ equation (3.23) leads to:

$$tf_{SC} = 1 + \frac{1}{\lambda(1-\xi_e)(1-\xi_i)} = 1 + tf_{SI}$$

Note that in general $tf^1_{SC} \neq tf^2_{SC}$.

3.4 Pump-Probe Experiment

In this section channel 1 references to an event that originates from the pump pulse and channel 2 if it originates from the probe pulse in a pump-probe experiment. Because the mean number of ionisation events is low the false coincidences are neglected. The probability that a coincidence originates from channel 1 can be calculated with (3.17) and (3.19):

$$P_1 = \frac{\lambda_1(1 + \lambda_1(1-\xi_e)(1-\xi_i))}{\lambda(1 + \lambda(1-\xi_e)(1-\xi_i))} \approx \frac{\lambda_1}{\lambda_1 + \lambda_2}$$

This leads to the result:

PROBABILITIE THAT A COINCIDENCE COUNT ORIGINATES FROM CHANNEL 1 (P_1) OR CHANNEL 2 (P_2)

$$P_1 \approx \frac{\lambda_1}{\lambda_1 + \lambda_2} \tag{3.25}$$

$$P_2 \approx \frac{\lambda_2}{\lambda_1 + \lambda_2} \tag{3.26}$$

3.5 Subtraction of Two Spectra

In this section the algorithm to subtract the pump-only spectrum from the pump-probe spectrum of one kind of molecule is derived. So the disentangling of the different spectra in the PEPICO measurement is already done. The algorithm estimates from the pump-only measurement the pump-only part in the pump-probe measurement and subtracts this from the pump-probe measurement (the pump-only part in the pump probe measurement is smaller than the pump-only measurement - this is explained in more detail in section 3.12). In figure 3.2 a schematic spectrum can be seen. For further calculations it is necessary to introduce some abbreviations:

- α $\cdots$ Counts from the pump-only measurement
- β $\cdots$ Counts from the pump-probe measurement
- $\beta 1$ $\cdots$ Counts from the pump pulse in the pump-probe measurement (channel 1)
- $\beta 2$ $\cdots$ Counts from the probe pulse in the pump-probe measurement (channel 2)
- L $\cdots$ Number of time bins

The spectrum of the pump-only measurement is described by the vector $\mathbf{n}_\alpha$, where the different vector entries represent the counts in a given time bin. The spectrum of the pump-probe measurement is described by $\mathbf{n}_\beta$. Therefore the total counts from the pump-only and pump-probe measurement are also known:

$$\sum_{\nu=1}^{L} n_{\alpha\nu} = N_\alpha \tag{3.27}$$

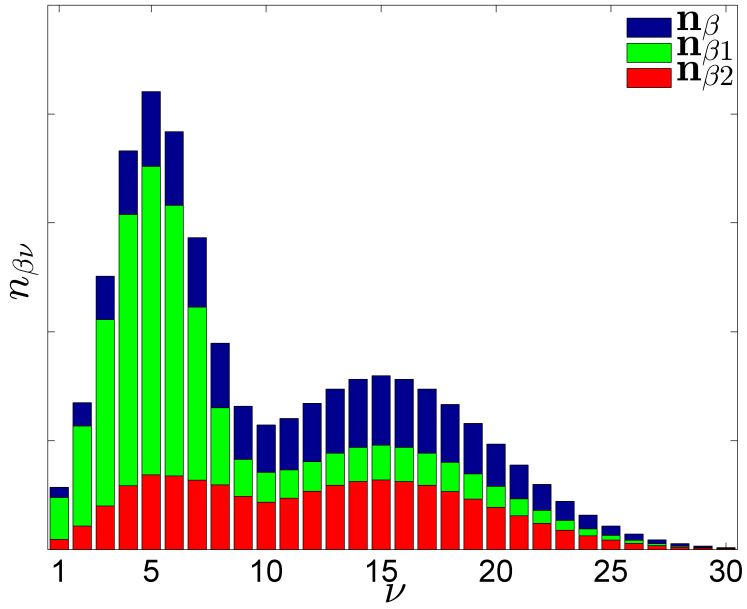

Figure 3.2: The TOF measures the flight time in discrete time intervals. The figure shows a schematic spectrum. For the calculation the value of a given time bin is not important. Therefore, the different time bins are numbered for better readability. The green spectrum is the estimated background and therefore the spectrum which originates from the pump pulses. For this estimation the background spectrum (pump-only) is used. The red spectrum is the spectrum which is created by the probe pulses. Note that the sum of the red and the green spectrum must be the blue (measured pump-probe) spectrum.

$$\sum_{\nu=1}^{L} n_{\beta\nu} = N_\beta \tag{3.28}$$

The total counts are abbreviated with the $\mathbf{N}$ vector: $\mathbf{N} = \begin{pmatrix} N_\alpha \\ N_\beta \end{pmatrix}$

To make calculations easier the probability that a count originates from the pump pulse ($P_{\beta 1}$) can be approximated with equation (3.25).

This information is enough to calculate the probability that the probe spectrum in the pump-probe experiment has a certain form $\mathbf{n}_{\beta 2}$:

$$p(\mathbf{n}_{\beta 2}|\mathbf{n}_\alpha, \mathbf{n}_\beta, \mathbf{N}, P_{\beta 1}) = \sum_{\mathbf{n}_{\beta 1}} \overbrace{p(\mathbf{n}_{\beta 2}|\mathbf{n}_\alpha, \mathbf{n}_\beta, \mathbf{N}, P_{\beta 1}, \mathbf{n}_{\beta 1})}^{\delta(\mathbf{n}_{\beta 1}+\mathbf{n}_{\beta 2}-\mathbf{n}_\beta)} p(\mathbf{n}_{\beta 1}|\mathbf{n}_\alpha, \mathbf{n}_\beta, \mathbf{N}, P_{\beta 1})$$
$$= p(\mathbf{n}_\beta - \mathbf{n}_{\beta 2}|\mathbf{n}_\alpha, \mathbf{n}_\beta, \mathbf{N}, P_{\beta 1}) \tag{3.29}$$

$p(\mathbf{n}_{\beta 2}|\mathbf{n}_\alpha, \mathbf{n}_\beta, \mathbf{N}, P_{\beta 1})$ is the same distribution as $p(\mathbf{n}_{\beta 1}|\mathbf{n}_\alpha, \mathbf{n}_\beta, \mathbf{N}, P_{\beta 1})$ but all axes are inverted and shifted by $\mathbf{n}_\beta$.

With the law of total probability $p(\mathbf{n}_{\beta 1}|\mathbf{n}_\alpha, \mathbf{n}_\beta, \mathbf{N}, P_{\beta 1})$ the total coincidence counts of the pump pulses $N_{\beta 1}$ and the probability that such a count is in time bin ν ($q_{1\nu}$) can be marginalized. Note that $\mathbf{q}_1$ is the spectral distribution.

$$p(\mathbf{n}_{\beta 1}|\mathbf{n}_\alpha, \mathbf{n}_\beta, \mathbf{N}, P_{\beta 1}) = \sum_{N_{\beta 1}=0}^{N_\beta} \int_0^1 \left(\prod_{\nu=1}^{L} dq_{1\nu} \right) p(\mathbf{n}_{\beta 1}|\mathbf{n}_\alpha, \mathbf{n}_\beta, \mathbf{N}, P_{\beta 1}, N_{\beta 1}, \mathbf{q}_1)$$
$$\times p(\mathbf{q}_1|\mathbf{n}_\alpha, \mathbf{n}_\beta, \mathbf{N}, P_{\beta 1}, N_{\beta 1}) p(N_{\beta 1}|\mathbf{n}_\alpha, \mathbf{n}_\beta, \mathbf{N}, P_{\beta 1}) \tag{3.30}$$

We identify the different distributions to:

- $\underline{p(N_{\beta 1}|\mathbf{n}_\alpha, \mathbf{n}_\beta, \mathbf{N}, P_{\beta 1})}$:

$p(N_{\beta 1}|\mathbf{n}_\alpha, \mathbf{n}_\beta, \mathbf{N}, P_{\beta 1})$ is a Binomial distribution because a coincidence originated from the pump or the probe pulse. The probability that a coincidence originated from the pump pulse is $P_{\beta 1}$.

$$p(N_{\beta 1}|\mathbf{n}_\alpha, \mathbf{n}_\beta, \mathbf{N}, P_{\beta 1}) = \binom{N_\beta}{N_{\beta 1}} P_{\beta 1}^{N_{\beta 1}} (1 - P_{\beta 1})^{N_\beta - N_{\beta 1}} = \binom{N_\beta}{N_{\beta 1}} \kappa^{N_{\beta 1}} (1 - P_{\beta 1})^{N_\beta}$$

With $\kappa = \frac{P_{\beta 1}}{1-P_{\beta 1}}$. Note that $(1 - P_{\beta 1})^{N_\beta} = \text{const}$.

- $\underline{p(\mathbf{q}_1|\mathbf{n}_\alpha, \mathbf{n}_\beta, \mathbf{N}, P_{\beta 1}, N_{\beta 1})}$:

The spectral information of the first channel can be calculated with the pump-only measurement and Bayes' theorem (the evidence is constant):

$$p(\mathbf{q}_1|\mathbf{n}_\alpha, \mathbf{n}_\beta, \mathbf{N}, P_{\beta 1}, N_{\beta 1}) \propto p(\mathbf{n}_\alpha|\mathbf{q}_1, \mathbf{n}_\beta, \mathbf{N}, P_{\beta 1}, N_{\beta 1}) p(\mathbf{q}_1|\mathbf{n}_\beta, \mathbf{N}, P_{\beta 1}, N_{\beta 1}) \tag{3.31}$$

The likelihood distribution is a Multinomial distribution:

$$p(\mathbf{n}_\alpha|\mathbf{q}_1,\mathbf{n}_\beta,\mathbf{N},P_{\beta1},N_{\beta1}) = N_\alpha!\prod_{\nu=1}^{L}\frac{q_\nu^{n_{\alpha\nu}}}{n_{\alpha\nu}!} \tag{3.32}$$

As the prior a Dirichlet distribution is used:

$$p(\mathbf{q}_1|\mathbf{n}_\beta,\mathbf{N},P_{\beta1},N_{\beta1}) \propto \delta\left(\sum_{\nu=1}^{L}q_\nu - 1\right)\prod_{\nu=1}^{L}q_\nu^{c_\nu-1} \tag{3.33}$$

The prior is flat if $c_\nu = 1 \ \ \forall\nu$. The advantage is that (3.32) multiplied by (3.33) is again shaped like (3.32) and therefore the calculation does not get more complicated but more flexible.

$$p(\mathbf{q}_1|\mathbf{n}_\alpha,\mathbf{n}_\beta,P_{\beta1},\mathbf{N},N_{\beta1}) \propto \delta\left(\sum_{\nu=1}^{L}q_{1\nu} - 1\right)\prod_{\nu=1}^{L}q_{1\nu}^{n_{\alpha\nu}+c_\nu-1} \tag{3.34}$$

- $\underline{p(\mathbf{n}_{\beta1}|\mathbf{n}_\alpha,\mathbf{n}_\beta,P_{\beta1},\mathbf{N},N_{\beta1},\mathbf{q}_1)}$:

The third distribution is a Multinomial distribution with the constraint $n_{\beta1\nu} \leq n_{\beta\nu} \ \ \forall\nu$:

$$p(\mathbf{n}_{\beta1}|\mathbf{n}_\alpha,\mathbf{n}_\beta,P_{\beta1},\mathbf{N},N_{\beta1},\mathbf{q}_1) = \delta\left(\sum_{\nu=1}^{L}n_{\beta1\nu} - N_{\beta1}\right)N_{\beta1}!\prod_{\nu=1}^{L}\Theta(n_{\beta1\nu}\leq n_{\beta\nu})\frac{q_{1\nu}^{n_{\beta1\nu}}}{n_{\beta1\nu}!} \tag{3.35}$$

With the heaviside step function Θ.

- $\underline{\text{Result}}$

Multiply everything together (with the conditions $\sum_{\nu=1}^{L}n_{\beta1\nu} = N_{\beta1}$ and $0 \leq n_{\beta1\nu} \leq n_{\beta\nu} \ \forall\nu$):

$$p(\mathbf{n}_{\beta1}|\mathbf{n}_\alpha,\mathbf{n}_\beta,P_{\beta1},\mathbf{N}) \propto \frac{\kappa^{N_{\beta1}}}{(N_\beta - N_{\beta1})!\prod_{\nu=1}^{L}n_{\beta1\nu}!}\underbrace{\int_0^1\left(\prod_{\nu=1}^{L}dq_{1\nu}\right)\delta\left(\sum_{\nu=1}^{L}q_{1\nu}-1\right)\prod_{\nu=1}^{L}q_{1\nu}^{n_\alpha+n_{\beta1\nu}+c_\nu-1}}_{=\frac{\prod_{\nu=1}^{L}\Gamma\left(n_{\alpha\nu}+n_{\beta1\nu}+c_\nu\right)}{\Gamma\left(\sum_{\nu=1}^{L}\left(n_{\alpha\nu}+n_{\beta1\nu}+c_\nu\right)\right)}}$$

The integral is the norm of the Dirichlet distribution and therefore a standard integral. Note that $\Gamma(x)$ is the gamma function.

Inserting this result in (3.29) gives the final result:

PROBABILITY FOR $\mathbf{n}_{\beta 2}$

$$p(\mathbf{n}_{\beta 2}|\mathbf{n}_\alpha, \mathbf{n}_\beta, P_{\beta 1}, \mathbf{N}) \propto \frac{\kappa^{-N_{\beta 2}}}{\Gamma\left(N_\alpha + N_\beta - N_{\beta 2} + C\right) N_{\beta 2}!} \prod_{\nu=1}^{L} \frac{\Gamma\left(n_{\alpha\nu} + n_{\beta\nu} - n_{\beta 2\nu} + c_\nu\right)}{(n_{\beta\nu} - n_{\beta 2\nu})!} \tag{3.36}$$

with

$$\kappa = \frac{\lambda_1}{\lambda_2} \tag{3.37}$$

$$\sum_{\nu=1}^{L} n_{\beta\nu} = N_\beta \tag{3.38}$$

$$\sum_{\nu=1}^{L} n_{\alpha\nu} = N_\alpha \tag{3.39}$$

$$\sum_{\nu=1}^{L} c_\nu = C \tag{3.40}$$

$$0 \leq n_{\beta 2\nu} \leq n_{\beta\nu} \ \forall \nu \tag{3.41}$$

3.6 Markov Chain Monte Carlo Metropolis Hastings Sampling

To calculate different moments of equation (3.36) it must be integrated. Unfortunately the term in front of the product couples the different time bins together and therefore makes it impossible to integrate the distribution analytically. However, the form of the distribution comes in handy because it is a big product of fractions of factorials (with $\Gamma(x+1) = x!$). This property makes the result well suited for Markov Chain Monte Carlo sampling (more precisely Metropolis Hastings algorithm - ref. [4]) where the probability for a step in the $\mathbf{n}_{\beta 2}$ space is the ratio of the probability of the new position to the probability of the old position (see figure 3.3):

$$p_{acc} = \min\left\{1, \frac{p(\mathbf{n}^f_{\beta 2})}{p(\mathbf{n}^i_{\beta 2})}\right\} \tag{3.42}$$

If the smallest possible Monte Carlo step is performed (add or subtract one count in one time bin) most of the terms cancel out. As a starting point in the $\mathbf{n}_{\beta 2}$ space every valid point can be used. The end result does not depend on the starting point if the result is converged. As a starting point the empty spectrum can be used where $n_{\beta 2\nu} = 0 \ \ \forall \nu$.

The basic idea of the Metropolis Hastings algorithm is that the distribution can be sampled if small steps are made in the probability space. The direction for the step is randomly chosen. The step is accepted every time if the probability of the new position is higher than the probability of the old one. If the probability function would be a landscape the Metropolis Hastings algorithm would always go uphill. If the new position has a lower probability than the current one the probability to accept this new position is smaller the smaller the fraction of the two probabilities is (eq. (3.42)) - this means that the algorithm goes sometimes downhill. This is necessary to sample the whole landscape and dont get stuck on a hill. The consequence is that the current position is most of the time on mountains and only rarely in valleys (but all mountains are visited). The disadvantage of the algorithm is that because of the small steps in probability space subsequent positions are highly correlated. However, the current position is not correlated to the position a few hundred/thousand/million steps earlier (number of steps depend on the problem).

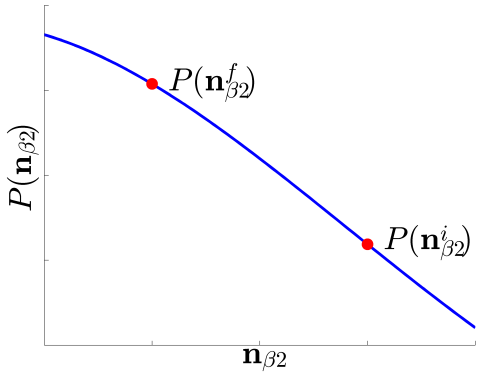

Figure 3.3: The probability to accept a Markov Chain Monte Carlo Metropolis Hastings step from the initial state $\mathbf{n}^i_{\beta 2}$ to the final state $\mathbf{n}^f_{\beta 2}$ is:
$p_{acc} = \min\left\{1, \frac{p(\mathbf{n}^f_{\beta 2})}{p(\mathbf{n}^i_{\beta 2})}\right\}$

MARKOV CHAIN MONTE CARLO ALGORITHM

Change $n_{\beta 2\mu} \to n_{\beta 2\mu} + 1$ (this leads to $N_{\beta 2} \to N_{\beta 2} + 1$).

$$\frac{p(\mathbf{n}^+_{\beta 2}|\mathbf{n}_\alpha, \mathbf{n}_\beta, P_{\beta 1}, \mathbf{N}^+)}{p(\mathbf{n}_{\beta 2}|\mathbf{n}_\alpha, \mathbf{n}_\beta, P_{\beta 1}, \mathbf{N})} = \frac{(n_{\beta\mu} - n_{\beta 2\mu})(N_\alpha + N_\beta - N_{\beta 2} + C - 1)}{\kappa(N_{\beta 2} + 1)(n_{\alpha\mu} + n_{\beta\mu} - n_{\beta 2\mu} + c_\mu - 1)} \tag{3.43}$$

Change $n_{\beta 2\mu} \to n_{\beta 2\mu} - 1$ (this leads to $N_{\beta 2} \to N_{\beta 2} - 1$).

$$\frac{p(\mathbf{n}^-_{\beta 2}|\mathbf{n}_\alpha, \mathbf{n}_\beta, P_{\beta 1}, \mathbf{N}^-)}{p(\mathbf{n}_{\beta 2}|\mathbf{n}_\alpha, \mathbf{n}_\beta, P_{\beta 1}, \mathbf{N})} = \frac{\kappa N_{\beta 2}(n_{\alpha\mu} + n_{\beta\mu} - n_{\beta 2\mu} + c_\mu)}{(n_{\beta\mu} - n_{\beta 2\mu} + 1)(N_\alpha + N_\beta - N_{\beta 2} + C)} \tag{3.44}$$

If a flat prior is used set $c_\nu = 1 \;\; \forall \nu \to C = L$. This steps can be performed under the condition $0 \leq n_{\beta 2\nu} \leq n_{\beta\nu}$.

Every view thousand steps the position in the spectrum space has to be stored. This positions are later used to calculate different moments of the distribution. At the end of the Monte Carlo run the convergence has to be checked. If the whole run is shorter than

about 100 times the biggest correlation time the calculated moments of the distribution can be false. To check convergence the binning algorithm is used (Ref. [4], S. 33ff). The basic idea of the binning algorithm is to take all the samples and create a new set of samples by taking the average over blocks of old samples (with block size N_B). Then calculate the standard error of this blocks. If the blocks are independent of each other the standard error stays constant. In fig. 3.4 a result of the binning algorithm is shown. For every time bin in the spectrum there is one curve. If the curves are nearly horizontal at the end the Monte Carlo run is converged.

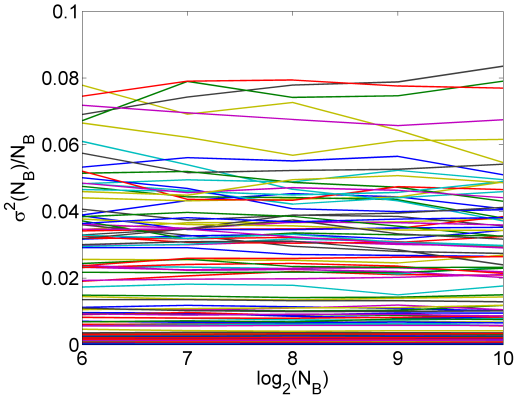

Figure 3.4: Result of the binning algorithm. Every line represents the Monte Carlo result of one time bin. The x-axis shows the size of one blocks (N_B) and the y-axis shows the square of the standard error. If the curves are approximately horizontal at the end then the Monte Carlo run is converged (like in this case). This means that the square of the standard error is independent of the block size. Note that a negative gradient is only due to lack of statistic.
File: *DiffPlotDataBayesTimedomain_3369*

3.7 Expectation Value and Covariance Matrix

To calculate different moments of the distribution (3.36) it must be sampled (f.ex. with Markov Chain Monte Carlo Metropolis Hastings). If the samples $\mathbf{n}^i_{\beta 2}$ are independent they can be used to approximate different integrals with Monte Carlo integration [13]. The index $\mathbf{n}^i_{\beta 2}$ represents the i-th sample.

$$\int_{-\infty}^{\infty} \mathbf{f}(\mathbf{n}_{\beta 2}) p(\mathbf{n}_{\beta 2}|\mathbf{n}_\alpha, \mathbf{n}_\beta, P_{\beta 1}, \mathbf{N}) d\mathbf{n}_{\beta 2} \approx \frac{1}{N} \sum_{i=1}^{N} \mathbf{f}(\mathbf{n}_{\beta 2}^i)$$

The most interesting features are the mean value and the covariance matrix. The covariance matrix contains information about the standard error (see later).

EXPECTATION VALUE AND COVARIANCE MATRIX

$$\langle \mathbf{n}_{\beta 2} \rangle \approx \frac{1}{N} \sum_{i=1}^{N} \mathbf{n}_{\beta 2}^i \tag{3.45}$$

$$C = \langle \Delta \mathbf{n}_{\beta 2} \Delta \mathbf{n}_{\beta 2}^T \rangle \approx \frac{1}{N} \sum_{i=1}^{N} \mathbf{n}_{\beta 2}^i \left(\mathbf{n}_{\beta 2}^i\right)^T - \langle \mathbf{n}_{\beta 2} \rangle \langle \mathbf{n}_{\beta 2}^T \rangle \tag{3.46}$$

It would also be possible to calculate $\langle \mathbf{q}_{\beta 2} \rangle$ but because $\sum_{\nu=1}^{L} \langle q_{\beta 2 \nu} \rangle = 1$ the relaxation of the population in the different states is not visible in $\langle \mathbf{q}_{\beta 2} \rangle$. Only the change in the spectral distribution would be visible.

3.8 Transform Data to a New Basis

This is necessary because the spectra are measured in flight time space and should be visualized for example in the electron energy space or ion mass space. In this section the variable of the new space is called E. Because of the basis change the measured values must be rescaled. Note that $n_{\beta 2 \nu} = n_{\beta 2}(t_\nu)$:

$$\tilde{n}_{\beta 2}(E_\nu) = \alpha n_{\beta 2}(t_\nu) \left| \frac{dt}{dE} \right|_{t_\nu} \tag{3.47}$$

$\left|\frac{dt}{dE}\right|$ is the Jacobian determinant. The factor α ensures that the sum over all $\tilde{n}(E_\nu)$ is the total sum of counts.

$$\alpha = \frac{\sum_{\nu=1}^{L} n_{\beta 2}(t_\nu)}{\sum_{\nu=1}^{L} n_{\beta 2}(t_\nu) \left|\frac{dt}{dE}\right|_{t_\nu}} \tag{3.48}$$

The Covariance matrix transforms like:

$$\tilde{C}_{\nu\mu} = C_{\nu\mu}\alpha^2 \left|\frac{dt}{dE}\right|_{t_\nu} \left|\frac{dt}{dE}\right|_{t_\mu} \tag{3.49}$$

3.9 Data Averaging

If data is averaged the standard error is reduced. For sake of readability $n_{\beta 2\nu}$ is now called n_ν.

The mean value s_i is defined as:

$$s_i = \frac{1}{N_i} \sum_{\nu \in i} n_\nu \tag{3.50}$$

with N_i the number of values that are averaged.

For the quantities of the mean value s Latin letters and for the quantities of n Greek letters are used. For example σ_ν^2 is the variance of n_ν and σ_i^2 the variance of s_i.

Since the expectation value operator $\langle x \rangle$ is linear, the expectation value of the mean value can be calculated very easily:

$$\langle s_i \rangle = \langle \frac{1}{N_i} \sum_{\nu \in i} n_\nu \rangle = \frac{1}{N_i} \sum_{\nu \in i} \langle n_\nu \rangle \tag{3.51}$$

The covariance matrix C_{ij} of the the mean values is:

$$C_{ij} = \langle \Delta s_i \Delta s_j \rangle = (\langle s_i s_j \rangle - \langle s_i \rangle \langle s_j \rangle)$$
$$= \frac{1}{N_i N_j} \sum_{\nu \in i} \sum_{\mu \in j} (\langle n_\nu n_\mu \rangle - \langle n_\nu \rangle \langle n_\mu \rangle) = \frac{1}{N_i N_j} \sum_{\nu \in i} \sum_{\mu \in j} C_{\nu\mu} \tag{3.52}$$

The diagonal elements of the covariance matrix are the variances:

$$\sigma_i^2 = C_{ii} = \frac{1}{N_i^2} \sum_{\nu \in i} \sum_{\mu \in i} C_{\nu\mu}$$

EXPECTATION VALUE AND COVARIANCE MATRIX OF AVERAGED DATA

$$s_i = \frac{1}{N_i} \sum_{\nu \in i} n_\nu \tag{3.53}$$

$$\langle s_i \rangle = \frac{1}{N_i} \sum_{\nu \in i} \langle n_\nu \rangle \tag{3.54}$$

$$C_{ij} = \frac{1}{N_i N_j} \sum_{\nu \in i} \sum_{\mu \in j} C_{\nu\mu} \tag{3.55}$$

$$\sigma_i^2 = C_{ii} = \frac{1}{N_i^2} \sum_{\nu \in i} \sum_{\mu \in i} C_{\nu\mu} = \frac{1}{N_i^2} \left(\sum_{\nu \in i} \sigma_\nu^2 + 2 \sum_{\nu \in i} \sum_{\substack{\mu \in i \\ \mu > \nu}} C_{\nu\mu} \right) \tag{3.56}$$

If data is integrated then N_i in equation (3.53) is 1 and therefore all N_i terms in equations (3.54) to (3.56) are 1.

3.10 Estimating λ_1 and λ_2 for Parent and Fragment in a PEPICO Measurement

The introduced algorithm estimates the expected spectrum of channel 2 if in the measurement channel 1 and 2 are measured at the same time and the contribution of channel 1 can be estimated in a separate experiment. Channel 1 refers to data that originate from the pump pulse and channel 2 refers to data that originate from the probe pulse. The different molecules are not distinguished in this algorithm. This means that it is necessary to estimate λ_1 and λ_2 for the parent ions (λ_1^p, λ_2^p) and for the fragment ions (λ_1^f, λ_2^f) separately. This is another approximation which can be done if the count rates are small and false coincidences are rare.

To estimate λ (parent or fragment), ξ_e and ξ_i at least three equations are needed. The formalism is described in Markus Bainschab's master thesis [1]. Here is a short summary:

1. **Equation**

   The probability to detect N_c coincidences if N_p laser pulses are fired at the molecules is binomial distributed:

$$p(N_c|\lambda,\xi_e,\xi_i,N_p) = \binom{N_p}{N_c} p(1,1|\lambda,\xi_e,\xi_i)^{N_c}(1-p(1,1|\lambda,\xi_e,\xi_i))^{N_p-N_c} \tag{3.57}$$

   The expectation value of the binomial distribution can be approximated with the measured coincidences N_c:

$$\begin{aligned}\langle N_c\rangle &= N_p p(1,1|\lambda,\xi_e,\xi_i)\\ &= N_p\lambda\xi_e\xi_i(1+\lambda(1-\xi_e)(1-\xi_i))e^{-\lambda(1-(1-\xi_e)(1-\xi_i))} \approx N_c\end{aligned} \tag{3.58}$$

2. and 3. **Equation**

   The probability to detect k_e electrons in a single laser pulse is Poisson distributed.

To see this the number of ionisation events n has to be marginalized:

$$\begin{aligned} p(k_e|\lambda,\xi_e,\xi_i) &= \sum_{n=k_e}^{\infty} p(k_e|\lambda,\xi_e,\xi_i,n)p(n|\lambda) \\ &= \sum_{n=k_e}^{\infty} \frac{n!}{(n-k_e)!k_e!}\xi_e^{k_e}(1-\xi_e)^{n-k_e}\frac{\lambda^n}{n!}e^{-\lambda} \\ &= \frac{(\lambda\xi_e)^{k_e}}{k_e!}e^{-\lambda}\sum_{n=k_e}^{\infty}\frac{(\lambda(1-\xi_e))^{n-k_e}}{(n-k_e)!} \\ &= \frac{(\lambda\xi_e)^{k_e}}{k_e!}e^{-\lambda\xi_e} \end{aligned} \tag{3.59}$$

The expectation value of the Poisson distribution is the negative value of the exponent of the exponential function namely $\lambda\xi_e$. This calculation is on the time scale of one laser shot. To compute the expected number of detected electrons in an experiment the time scale must be rescaled. This is done by multiplying λ and k_e by N_p. Then the expected number of detected electrons in the experiment is:

$$N_p\langle k_e\rangle = N_p\lambda\xi_e \approx n_e \tag{3.60}$$

Or rewritten:

$$\langle k_e\rangle = \lambda\xi_e \approx \frac{n_e}{N_p} \tag{3.61}$$

The same is true for the ions:

$$\langle k_i\rangle = \lambda\xi_i \approx \frac{n_i}{N_p} \tag{3.62}$$

Insert equation (3.61) and (3.62) in (3.58) gives:

$$\frac{n_e n_i}{\lambda N_p}\left(1+\lambda\left(1-\frac{n_e}{\lambda N_p}\right)\left(1-\frac{n_i}{\lambda N_p}\right)\right)e^{-\lambda\left(1-\left(1-\frac{n_e}{\lambda N_p}\right)\left(1-\frac{n_i}{\lambda N_p}\right)\right)} = N_c \tag{3.63}$$

This equation only depends on λ and measured values. With λ it is possible to calculate the detection probabilities with equations (3.61) and (3.62).

ESTIMATE λ, ξ_e AND ξ_i

Solve for λ:

$$\frac{n_e n_i}{\lambda N_p}\left(1+\lambda\left(1-\frac{n_e}{\lambda N_p}\right)\left(1-\frac{n_i}{\lambda N_p}\right)\right)e^{-\lambda\left(1-\left(1-\frac{n_e}{\lambda N_p}\right)\left(1-\frac{n_i}{\lambda N_p}\right)\right)}=N_c \tag{3.64}$$

with:
$n_e \cdots$ total measured electrons
$n_e \cdots$ total measured ions
$N_c \cdots$ total measured coincidences
$N_p \cdots$ total number of laser pulses

$$\xi_e \approx \frac{n_e}{\lambda N_p} \tag{3.65}$$

$$\xi_i \approx \frac{n_i}{\lambda N_p} \tag{3.66}$$

3.11 Estimate κ in an Electron Mode Measurement

If only electrons are detected $P_{\beta 1}$ and therefore κ (cf., eq. (3.37)) can be directly estimated without estimating ξ_e or ξ_i. α represents only channel 1 is active (background) and β represent channel 1 and 2 are active:

ESTIMATE κ IN AN ELECTRON MODE MEASUREMENT

$$\kappa = \frac{P_{\beta 1}}{1 - P_{\beta 1}} \tag{3.67}$$

$$P_{\beta 1} \approx \frac{\lambda_1}{\lambda_1 + \lambda_2} \frac{N_p \xi_e}{N_p \xi_e} \approx \frac{n_e^\alpha}{n_e^\beta} \tag{3.68}$$

3.12 Comparison Bayes' Subtraction with Simple Subtraction

3.12.1 Estimating the Total Count Difference

Equation (3.17) shows that in a pump-probe measurement there are four possibilities to detect a coincidence in a single laser shot:

$$\begin{aligned} p(1,1|\lambda_1,\lambda_2,\xi_e,\xi_i) = {} & p(1,1|\lambda_1,\xi_e,\xi_i)p(0,0|\lambda_2,\xi_e,\xi_i) + p(0,0|\lambda_1,\xi_e,\xi_i)p(1,1|\lambda_2,\xi_e,\xi_i) \\ & + p(1,0|\lambda_1,\xi_e,\xi_i)p(0,1|\lambda_2,\xi_e,\xi_i) + p(0,1|\lambda_1,\xi_e,\xi_i)p(1,0|\lambda_2,\xi_e,\xi_i) \end{aligned}$$

Due to a small $\lambda = \lambda_1 + \lambda_2$ the false coincidences are neglectable:

$$p(1,1|\lambda_1,\lambda_2,\xi_e,\xi_i) \approx p(1,1|\lambda_1,\xi_e,\xi_i)p(0,0|\lambda_2,\xi_e,\xi_i) + \overbrace{p(0,0|\lambda_1,\xi_e,\xi_i)p(1,1|\lambda_2,\xi_e,\xi_i)}^{p_2}$$

In the pump-probe experiment the probability for a coincidence that originates from channel 2 is p_2.
If the background ($p(1,1|\lambda_1,\xi_e,\xi_i)$) is simply subtracted from the equation above the result is:

$$\begin{aligned} & p(1,1|\lambda_1,\lambda_2,\xi_e,\xi_i) - p(1,1|\lambda_1,\xi_e,\xi_i) \approx \\ & \underbrace{(p(0,0|\lambda_2,\xi_e,\xi_i) - 1)p(1,1|\lambda_1,\xi_e,\xi_i)}_{\Delta p \leq 0} + p_2 \end{aligned} \tag{3.69}$$

This equation differs from the real probability that a coincidence originates from channel 2 by Δp. Note that Δp is negative and its absolute value increases as λ_2 grows (and

therefore $p(0,0|\lambda_2,\xi_e,\xi_i)$ gets smaller). This means that the simple subtraction subtract too much total counts and the error increases if the signal of channel 2 increases. The solution would be to rescale $p(1,1|\lambda_1,\xi_e,\xi_i)$ with χ before the subtraction such that Δp vanishes:

$$\begin{aligned} &p(1,1|\lambda_1,\lambda_2,\xi_e,\xi_i) - \chi p(1,1|\lambda_1,\xi_e,\xi_i) \approx \\ &\underbrace{(p(0,0|\lambda_2,\xi_e,\xi_i) - \chi)}_{\stackrel{!}{=}0} p(1,1|\lambda_1,\xi_e,\xi_i) + p_2 \end{aligned} \tag{3.70}$$

The scaling factor χ is therefore:

$$\chi = p(0,0|\lambda_2,\xi_e,\xi_i) = e^{-\lambda_2(1-(1-\xi_e)(1-\xi_i))} \tag{3.71}$$

This estimation is only for the total coincidence counts in a measurement. There is no spectral information in it.

Another point of view is shown in figure 3.5: If in the pump-probe measurement a molecule is ionized from the pump pulse this ionization event would belong to the background signal. However, if the probe pulse also ionizes a molecule this event is not a one to one coincidence. This means that the probability to get a pump coincidence is in the pump-probe measurement less likely.

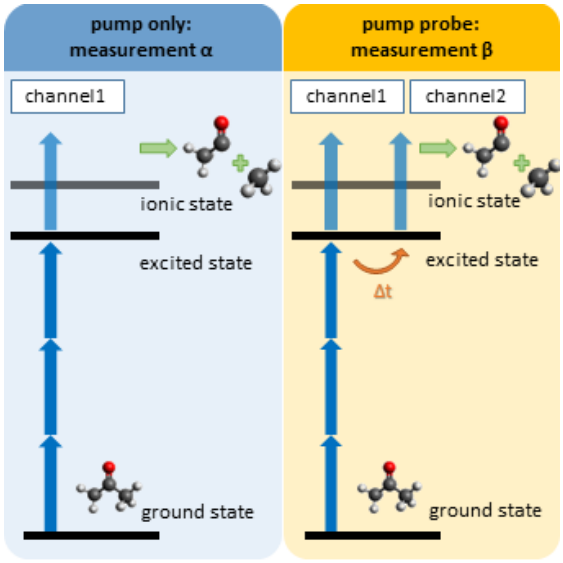

Figure 3.5: If in the pump-probe measurement a molecule is ionized from the pump pulse this ionization event would belong to the background signal. However, if the probe pulse also ionizes a molecule this event is not a one to one coincidence. This means that the probability to get a pump coincidence is in the pump-probe measurement less likely.

3.12.2 Comparing Spectra

To check the difference of the simple subtraction and the Markov Chain Monte Carlo subtraction two extreme chases are compared. A measurement at the overlap (0 fs time delay) and a measurement far away from the overlap (1000 fs time delay). The main advantages with the Markov Chain Monte Carlo subtraction is a reduction of the noise and the ability to draw error bands which make interpretation of the data much easier.

0 fs Time Delay

Figure 3.6 shows no real difference between the direct subtraction and the Monte Carlo subtraction method. The total signal in figure 3.6e is bigger than in figure 3.6c which is discussed in section 3.12.1. The error bands are very small and can not be seen in figure 3.6e and 3.6f because the signal from the probe pulse in the pump probe measurement is very dominant.

1000 fs Time Delay

At high delays and low count rates the Monte Carlo subtraction method shows its strength. Very noisy signals are much smoother and error bands make interpretation much easier. The very noisy signal for example in figure 3.7c is much smoother in 3.7e. The information of the noise is now shown in the error bands. Also, the noise in figure 3.7c at about 2.5 eV is nearly as big as the structure at 0.7 eV. The structure is significant because there the overall signal in figure 3.7a is much smaller and therefore the noise. Also, in figure 3.7d it is hard to interpret if there are two big energy bands from 0 eV to about 1.2 eV and from 1.2 eV to 3 eV. But in figure 3.7f it is clear that there are not two separated energy bands.

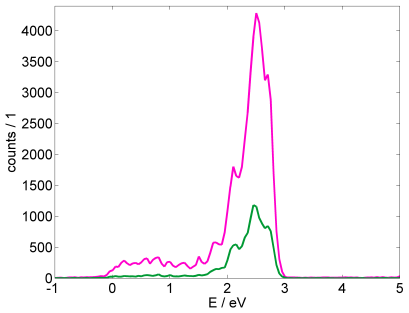

(a) Parent spectrum
Pink: Pump-probe measurement
Green: Pump-only measurement (background)

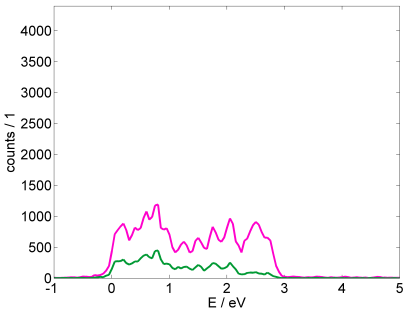

(b) Fragment spectrum
Pink: Pump-probe measurement
Green: Pump-only measurement (background)

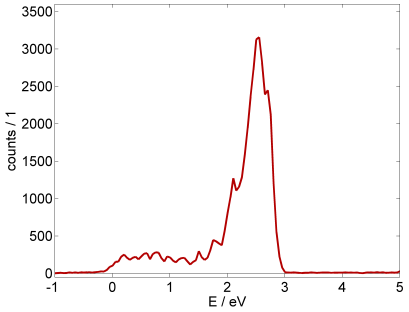

(c) Parent spectrum: Difference between pump-probe measurement and pump-only measurement

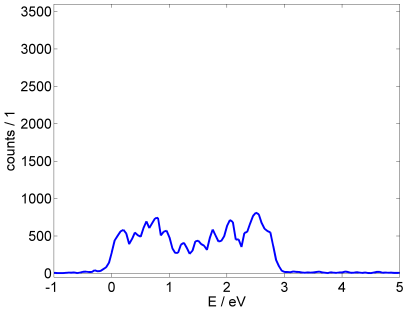

(d) Fragment spectrum: Difference between pump-probe measurement and pump-only measurement

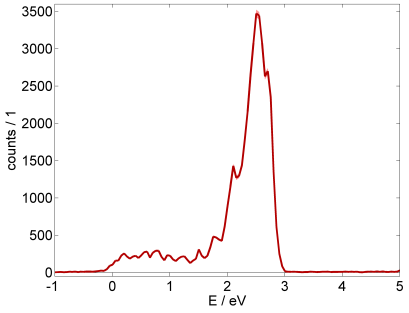

(e) Parent spectrum: Markov Chain Monte Carlo difference between pump-probe measurement and pump-only measurement

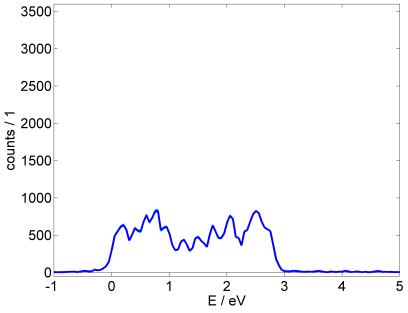

(f) Fragment spectrum: Markov Chain Monte Carlo difference between pump-probe measurement and pump-only measurement

Figure 3.6: Pump-probe spectra at 0 fs delay. The direct subtracted spectra look similar to the Markov Chain Monte Carlo subtracted spectra. Due to the high signal increase in the pump-probe measurement the signal-to-noise ratio is very good. Clear structures are visible. The error bands in the Monte Carlo spectra are not visible because they are so small. The only difference: The parent spectrum of the Monte Carlo subtraction is higher in amplitude. This phenomenon is discussed in subsection 3.12.1.
Pump-probe measurement: *eiTOF_3359*
Pump-only measurement: *eiTOF_3360*

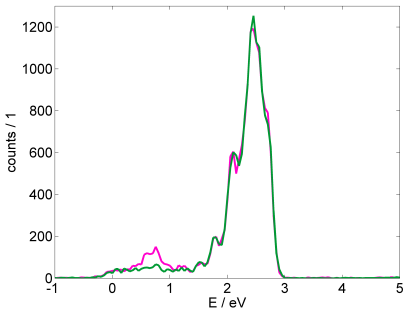

(a) Parent spectrum
Pink: Pump-probe measurement
Green: Pump-only measurement (background)

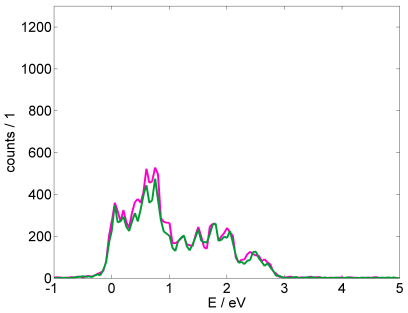

(b) Fragment spectrum
Pink: Pump-probe measurement
Green: Pump-only measurement (background)

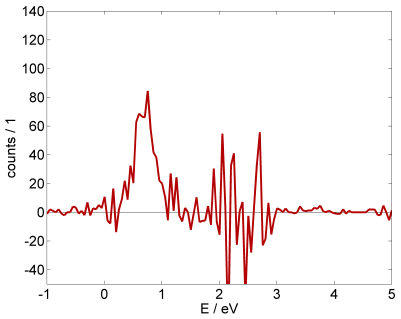

(c) Parent spectrum: Difference between pump-probe measurement and Pump only measurement

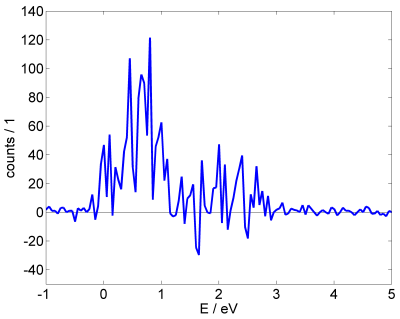

(d) Fragment spectrum: Difference between pump-probe measurement and pump-only measurement

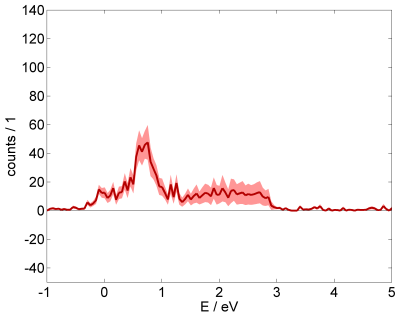

(e) Parent spectrum: Markov Chain Monte Carlo difference between pump-probe measurement and pump-only measurement

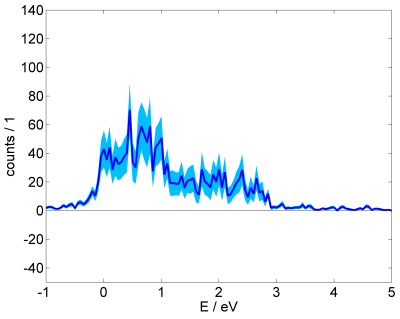

(f) Fragment spectrum: Markov Chain Monte Carlo difference between pump-probe measurement and pump-only measurement

Figure 3.7: Pump-probe spectra at 1000 fs delay. The direct subtracted spectra are very noisy. In figure (c) the noise at about 2.5 eV is nearly as big as the structure at around 0.7 eV. Without the original spectrum (a) the interpretation is difficult because the noise amplitude is related to the signal height. Higher signals have a higher absolute noise. Overall the direct subtracted spectra are hard to interpret. Note that negative signals are impossible and only a result of noise. The Monte Carlo spectra are less noisy and there is no negative signal. The very spiky signal in (c) is much smoother with broad error bands in (e) - there are no significant structures above 1.2 eV.
Pump-probe measurement: *eiTOF_3408*
Pump-only measurement: *eiTOF_3409*

CHAPTER 4

Pump-Probe Result

4.1 Fit Model

A classical three state decay model is used where state $|1\rangle$ decays into state $|2\rangle$ and a dark state $|d\rangle$ and state $|2\rangle$ also decays into the dark state $|d\rangle$ (see fig. 4.1). The decay of the population in a certain state is proportional to the population of the state.

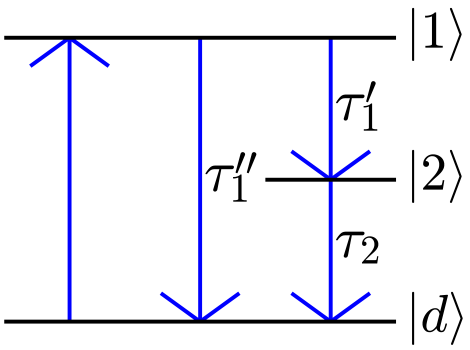

Figure 4.1: Schematic drawing of a three state System. A certain population of electrons is excited from a dark state $|d\rangle$ to an excited state $|1\rangle$ and decays with a time constant of τ_1' into state $|2\rangle$ and with a time constant of τ_1'' into a dark state. The population in state $|2\rangle$ also decay with a time constant of τ_2 into a dark state.

4.1.1 Solving linear differential equations with Greens functions

A typical linear differential equation can be written with a linear differential operator D that acts on a function $y(t)$ which is equal to an inhomogeneity $f(t)$:

$$D[y(t)] = f(t) \tag{4.1}$$

Because the linear differential operator is by definition linear, a rescaling of $y(t)$ (with scaling factor a which depends not on t) can be rewritten to a scaling of D:

$$D[a \cdot y(t)] = a \cdot D[y(t)] \tag{4.2}$$

Another property of linearity is that if the differential operator acts on a sum of functions it is the same as if the differential operator acts on every function separately and then the result is added together:

$$D\left[\sum_i y_i(t)\right] = \sum_i D\left[y_i(t)\right] \tag{4.3}$$

The Greens function $G(t)$ describes how the system described by D reacts on a delta shaped inhomogeneity. Therefore, the Greens function is also called *impulse response function*:

$$D[G(t)] = \delta(t) \tag{4.4}$$

The function $y(t)$ can be calculated as a convolution of the Greens function $G(t)$ with the inhomogeneity $f(t)$:

$$y(t) = \int_{-\infty}^{\infty} G(t-t')f(t')dt' \tag{4.5}$$

Proof:

$$D[y(t)] = D\left[\int_{-\infty}^{\infty} G(t-t')f(t')dt'\right] = \int_{-\infty}^{\infty} \underbrace{D[G(t-t')]}_{\delta(t-t')} f(t')dt' = f(t) \tag{4.6}$$

Note that the Greens function only depends on D (the system) and not on the inhomogeneity $f(t)$.

4.2 Greens Function of an Unstable State

The decay of the population $N(t)$ of an unstable state shall be proportional to the population:

$$D[N] = \dot{N} + \frac{N}{\tau} \tag{4.7}$$

To calculate the Greens function equation (4.1) and (4.7) are Fourier transformed:

$$-i\omega G(\omega) + \frac{G(\omega)}{\tau} = 1 \tag{4.8}$$

solve for $G(\omega)$:

$$G(\omega) = \frac{1}{-i\omega + \frac{1}{\tau}} \tag{4.9}$$

Inverse Fourier transform equation (4.9) leads to (with $\tau \in R^+$):

GREENSFUNCTION OF EXPONENTIAL DECAY DIFFERENTIAL EQUATION
$$G(t) = \Theta(t)e^{-\frac{t}{\tau}} \tag{4.10}$$

The Greens function is an exponential decay multiplied by the heaviside step function. The state is empty before $t = 0$ and is filled at $t = 0$. After $t = 0$ the state exponentially decays.

4.3 Fill First State with a Gaussian:

The state shall be filled with a Gaussian shaped inhomogeneity. In the experiment the pump pulse intensity I over time is shaped approximately like a Gaussian and the multi photon absorption probability p is proportional to the pulse intensity to the power of the number of photons N used for the absorption ($p \propto I^N$ [7]), which is again Gaussian shaped.

The Gaussian shall have an area of N_0. This means that the Gaussian excites N_0 molecules to the state $|1\rangle$:

$$f(t;\sigma) = \frac{N_0}{\sqrt{2\pi\sigma^2}} e^{-\frac{t^2}{2\sigma^2}} \tag{4.11}$$

State $|1\rangle$ decays with two different time constants. The differential equation of the system is:

$$N + \dot{N}\left(\frac{1}{\tau'} + \frac{1}{\tau''}\right) = \dot{N} + \frac{N}{\tau} = f(t;\sigma) \tag{4.12}$$

Use equation (4.5) and (4.10) to calculate $N(t)$:

$$\begin{aligned}
\frac{N(t;\tau,\sigma)}{N_0} &= \int_{-\infty}^{t} e^{-\frac{t-t'}{\tau_1}} \frac{1}{\sqrt{2\pi\sigma^2}} e^{-\frac{t'^2}{2\sigma^2}} dt' \\
&= \frac{1}{\sqrt{2\pi\sigma^2}} e^{-\frac{t}{\tau_1}} \int_{-\infty}^{t} e^{-\frac{t'^2 - 2t'\frac{\sigma^2}{\tau_1} + \left(\frac{\sigma^2}{\tau_1}\right)^2 - \left(\frac{\sigma^2}{\tau_1}\right)^2}{2\sigma^2}} dt' \\
&= \frac{1}{\sqrt{2\pi\sigma^2}} e^{-\frac{t}{\tau_1}} e^{\frac{\sigma^2}{2\tau_1^2}} \int_{-\infty}^{t} e^{-\frac{(t'-\frac{\sigma^2}{\tau_1})}{2\sigma^2}} dt' \\
&= \frac{1}{\sqrt{2\pi\sigma^2}} e^{-\frac{t}{\tau_1}} e^{\frac{\sigma^2}{2\tau_1^2}} \sqrt{2}\sigma \int_{-\infty}^{\frac{(t-\frac{\sigma^2}{\tau_1})}{\sqrt{2}\sigma}} e^{-t'^2} dt' \\
&= \frac{1}{\sqrt{\pi}} e^{-\frac{t}{\tau_1}} e^{\frac{\sigma^2}{2\tau_1^2}} \frac{\sqrt{\pi}}{2} \left(2 - \operatorname{erfc}\left(\frac{(t-\frac{\sigma^2}{\tau_1})}{\sqrt{2}\sigma}\right)\right) \\
&= \frac{1}{2} e^{-\frac{t}{\tau_1}} e^{\frac{\sigma^2}{2\tau_1^2}} \left(2 - \operatorname{erfc}\left(\frac{(t-\frac{\sigma^2}{\tau_1})}{\sqrt{2}\sigma}\right)\right)
\end{aligned}$$

with

$$\begin{aligned}
&\operatorname{erfc}(t) = \frac{2}{\sqrt{\pi}} \int_t^{\infty} e^{-x^2} dx \\
&\operatorname{erfc}(-\infty) = 2 \\
&\operatorname{erfc}(\infty) = 0
\end{aligned}$$

Final result:

POPULATION OF A STATE FILLED WITH A GAUSSIAN

$$N(t;\tau_1,\sigma,N_0) = \frac{N_0}{2} e^{\frac{\sigma^2}{2\tau_1^2}} \left(2 - \operatorname{erfc}\left(\frac{t-\frac{\sigma^2}{\tau_1}}{\sqrt{2}\sigma}\right)\right) e^{\frac{-t}{\tau_1}} \tag{4.13}$$

$$\frac{1}{\tau_1} = \frac{1}{\tau_1'} + \frac{1}{\tau_1''} \tag{4.14}$$

The term:

$$\frac{1}{2}\left(2 - \operatorname{erfc}\left(\frac{t-\frac{\sigma^2}{\tau_1}}{\sqrt{2}\sigma}\right)\right) \tag{4.15}$$

is 0 at $t = -\infty$ and changes its value around $t = \frac{\sigma^2}{\tau_1}$ to 1. σ describes how fast this change happens. Note that the Gaussian function which fills state $|1\rangle$ is centred at $t = 0$ but the change in population is shifted by $\frac{\sigma^2}{\tau_1}$. The factor $e^{-\frac{t}{\tau_1}}$ is 1 at $t = 0$ the smaller τ_1 is the steeper is the exponential function. To counter the big values of the exponential function below $t = 0$ the function (4.15) is shifted towards a higher t so that the product of (4.15) and the exponential function is small again. The prefactor $e^{\frac{\sigma^2}{2\tau_1^2}}$ normalizes $N(t;\tau_1,\sigma,N_0)$ so that the total population that passes through the state is N_0.

4.4 Fill the Second State with the Decay of the First State

$N_1(t) = N(t;\tau_1,\sigma,N_0)$ and N_1 decays in a state N_2 which also decays like (4.7). In this case the inhomogeneity of N_2 is $\frac{N_1}{\tau_1'}$ because this term in equation (4.12) describes the decay of the state N_1 into the state N_2. To calculate the population of N_2 again (4.5) and (4.10) are used. For the derivation $\tilde{N}_1 = \text{const} \cdot N_1$ is used and the abbreviations $A = \sqrt{2}\sigma$ and $C = \frac{\sigma}{\sqrt{2}\tau_1}$ are introduced to simplify the equations:

$$\tilde{N}_1(t) = 2e^{-\frac{\sigma^2}{2\tau_1^2}} \frac{N_1(t)}{N_0} = e^{-\frac{t}{\tau_1}} \left[2 - \operatorname{erfc}\left(\frac{t}{A} + C\right)\right] \tag{4.16}$$

Calculate:

$$\tilde{N}_2(t) = \int_{-\infty}^{t} e^{-\frac{t-t'}{\tau_2}} \frac{\tilde{N}_1(t')}{\tau_1'} dt' \tag{4.17}$$

Note that

$$\tilde{N}_2(t) = 2e^{-\frac{\sigma^2}{2\tau_1^2}} \frac{N_2(t)}{N_0} \tag{4.18}$$

In the special case of $\tau_1 = \tau_2 = \tau$ equation (4.17) has a different form because the exponential function in the integral vanishes.

First take a look at the special case:

$$\begin{aligned}
\tilde{N}_2(t) &= \frac{e^{-\frac{t}{\tau}}}{\tau_1'} \int_{-\infty}^{t} \left(2 - \operatorname{erfc}\left(\frac{t'}{A} + C\right)\right) dt' \\
&= A\frac{e^{-\frac{t}{\tau}}}{\tau_1'} \int_{-\infty}^{\frac{t}{A}+C} \left(2 - \operatorname{erfc}(t')\right) dt' \\
&= A\frac{e^{-\frac{t}{\tau}}}{\tau_1'} \left(t' \left(2 - \operatorname{erfc}(t')\right) |_{-\infty}^{\frac{t}{A}+C} - \frac{2}{\sqrt{\pi}} \int_{-\infty}^{\frac{t}{A}+C} t' e^{-t'^2} dt' \right) \\
&= A\frac{e^{-\frac{t}{\tau}}}{\tau_1'} \left(t' \left(2 - \operatorname{erfc}(t')\right) |_{-\infty}^{\frac{t}{A}+C} - \frac{1}{\sqrt{\pi}} \left(\int_{\infty}^{\left(\frac{t}{A}+C\right)^2} e^{-t'} dt' \right) \right) \\
&= A\frac{e^{-\frac{t}{\tau}}}{\tau_1'} \left(\left(\frac{t}{A} + C\right) \left(2 - \operatorname{erfc}\left(\frac{t}{A} + C\right)\right) + \frac{e^{-(\frac{t}{A}+C)^2}}{\sqrt{\pi}} \right)
\end{aligned} \tag{4.19}$$

The integral was solved with partial integration and:

$$\frac{d}{dt}\operatorname{erfc}(t) = -\frac{2}{\sqrt{\pi}} e^{-t^2} \tag{4.20}$$

$N_2(t)$ can be calculated with equation (4.18) and (4.19) and the abbreviations $A = \sqrt{2}\sigma$ and $C = -\frac{\sigma}{\sqrt{2}\tau}$:

$$N_2(t) = \frac{N_0\sigma}{\sqrt{2}\tau_1'} e^{\frac{\sigma^2}{2\tau^2}} \left[\frac{t-\frac{\sigma^2}{\tau}}{\sqrt{2}\sigma} \left(2 - \operatorname{erfc}\left(\frac{t-\frac{\sigma^2}{\tau}}{\sqrt{2}\sigma} \right) \right) + \frac{1}{\sqrt{\pi}} e^{-\frac{\left(t-\frac{\sigma^2}{\tau}\right)^2}{2\sigma^2}} \right] e^{-\frac{t}{\tau}}$$
$$= \frac{t-\frac{\sigma^2}{\tau}}{\tau_1'} N_1(t) + \frac{N_0\sigma}{\sqrt{2\pi}\tau_1'} e^{-\frac{t^2}{2\sigma^2}} \tag{4.21}$$

Now look at the case if $\tau_1 \neq \tau_2$:

Introduce the abbreviation $B = \frac{1}{\tau_1} - \frac{1}{\tau_2}$:

$$\tilde{N}_2(t) = e^{-\frac{t}{\tau_2}} \frac{1}{\tau_1'} \left[\int_{-\infty}^{t} e^{-t'B} \left(2 - \operatorname{erfc}\left(\frac{t'}{A} + C \right) \right) dt' \right]$$
$$= e^{-\frac{t}{\tau_2}} \frac{1}{B\tau_1'} \left[\underbrace{- e^{-t'B} \left(2 - \operatorname{erfc}\left(\frac{t'}{A} + C \right) \right) |_{-\infty}^{t}}_{e^{-tB}\left(2-\operatorname{erfc}\left(\frac{t}{A}+C\right)\right)} + \frac{2}{A\sqrt{\pi}} \underbrace{\int_{-\infty}^{t} e^{-Bt'} e^{-\left(\frac{t}{A}+C\right)} dt'}_{I} \right]$$

Again partial integration is used. Solve the integral I:

$$\int_{-\infty}^{t} e^{-\left(\frac{t'}{A}+C\right)^2 - t'B} dt' = \int_{-\infty}^{t} e^{-\left(\left(\frac{t'}{A}\right)^2 + t'\left(B+2\frac{C}{A}\right) + C^2 + \left(\frac{AB}{2}+C\right)^2 - \left(\frac{AB}{2}+C\right)^2 \right)} dt'$$
$$= e^{\left(\frac{AB}{2}\right)^2 + ABC} \int_{-\infty}^{t} e^{-\left(\frac{t'}{A}+\frac{AB}{2}+C\right)^2} dt'$$
$$= A\frac{\sqrt{\pi}}{2} e^{\left(\frac{AB}{2}\right)^2 + ABC} \left(2 - \operatorname{erfc}\left(\frac{t}{A} + \frac{BA}{2} + C \right) \right)$$

Add all terms together:

$$\tilde{N}_2(t) = e^{-\frac{t}{\tau_2}} \frac{1}{B\tau_1'} \left[e^{\left(\frac{AB}{2}\right)^2 + ABC} \left(2 - \operatorname{erfc}\left(\frac{t}{A} + \frac{BA}{2} + C \right) \right) - \left(2 - \operatorname{erfc}\left(\frac{t}{A} + C \right) \right) e^{-tB} \right]$$
$$= \frac{1}{B\tau_1'} \left[e^{\left(\frac{AB}{2}\right)^2 + ABC} \left[2 - \operatorname{erfc}\left(\frac{t}{A} + \frac{BA}{2} + C \right) \right] e^{-\frac{t}{\tau_2}} - \underbrace{\left[2 - \operatorname{erfc}\left(\frac{t}{A} + C \right) \right] e^{-\frac{t}{\tau_1}}}_{\tilde{N}_1(t)} \right]$$

with $A = \sqrt{2}\sigma$, $B = \frac{1}{\tau_1} - \frac{1}{\tau_2}$ and $C = -\frac{\sigma}{\sqrt{2}\tau_1}$ the exponential constant reduces to:

$$
\begin{aligned}
e^{\left(\frac{AB}{2}\right)^2+ABC} &= e^{\frac{\sigma^2}{2}\left(\frac{1}{\tau_1}-\frac{1}{\tau_2}\right)^2-\frac{\sigma^2}{\tau_1}\left(\frac{1}{\tau_1}-\frac{1}{\tau_2}\right)} \\
&= e^{\sigma^2\left(\frac{1}{2\tau_1^2}+\frac{1}{2\tau_2^2}-\frac{1}{\tau_1\tau_2}-\frac{1}{\tau_1^2}+\frac{1}{\tau_1\tau_2}\right)} \\
&= e^{\sigma^2\left(\frac{1}{2\tau_2^2}-\frac{1}{2\tau_1^2}\right)}
\end{aligned}
$$

and with (4.18) the result gets

$$
N_2(t) = \frac{1}{\frac{\tau_1'}{\tau_1}\left(1-\frac{\tau_1}{\tau_2}\right)}\left[\underbrace{\frac{N_0}{2}e^{\frac{\sigma^2}{2\tau_2^2}}\left[2-\operatorname{erfc}\left(\frac{t-\frac{\sigma^2}{\tau_2}}{\sqrt{2}\sigma}\right)\right]e^{-\frac{t}{\tau_2}}}_{N(t;\tau_2,\sigma,N_0)}-N_1(t)\right] \tag{4.22}
$$

In summery the fit model for the first and second state which is filled with a Gaussian is:

POPULATION OF A STATE FILLED WITH A GAUSSIAN

State $|1\rangle$ is filled with a Gaussian

$$f(t;\sigma) = \frac{N_0}{\sqrt{2\pi\sigma^2}} e^{-\frac{t^2}{2\sigma^2}} \tag{4.23}$$

Population of state $|1\rangle$:

$$N_1(t) = N(t;\tau_1,\sigma,N_0) \tag{4.24}$$

Population of state $|2\rangle$ ($\tau_1 \neq \tau_2$):

$$N_2(t) = \frac{\tau_1}{\tau_1'} \frac{N(t;\tau_2,\sigma,N_0) - N(t;\tau_1,\sigma,N_0)}{1-\frac{\tau_1}{\tau_2}} \tag{4.25}$$

Population of state $|2\rangle$ ($\tau_1 = \tau_2 = \tau$):

$$N_2(t) = \frac{t-\frac{\sigma^2}{\tau}}{\tau_1'} N(t;\tau,\sigma,N_0) + \frac{\sigma^2}{\tau_1'} f(t;\sigma) \tag{4.26}$$

with

$$N(t;\tau,\sigma,N_0) = \frac{N_0}{2} e^{\frac{\sigma^2}{2\tau^2}} \left(2 - \operatorname{erfc}\left(\frac{(t-\frac{\sigma^2}{\tau})}{\sqrt{2}\sigma}\right)\right) e^{\frac{-t}{\tau}} \tag{4.27}$$

$$\frac{1}{\tau_1} = \frac{1}{\tau_1'} + \frac{1}{\tau_1''} \tag{4.28}$$

The temporal behaviour of the population of state $|2\rangle$ does not depend on τ_1' but only on τ_1. The only effect of τ_1' on the population of state $|2\rangle$ is the amplitude.

In the extreme case of $\sigma \to 0$ equation (4.27) simplifies to:

$$N(t;\tau,\sigma,N_0) = \Theta(t) N_0 e^{\frac{-t}{\tau}} \tag{4.29}$$

With the heaviside step function $\Theta(t)$.

If additionally state $|1\rangle$ decays only in state $|2\rangle$ ($\tau'' = \infty \rightarrow \tau_1' = \tau_1$) then the sum of the population in state $|1\rangle$ and state $|2\rangle$ becomes to:

$$N_1(t) + N_2(t) = \Theta(t) N_0 \left(e^{-\frac{t}{\tau_1}} + \frac{\tau_2}{\tau_2 - \tau_1} \left(e^{-\frac{t}{\tau_2}} - e^{-\frac{t}{\tau_1}} \right) \right) \tag{4.30}$$

This equation is used for example by the group of Stolow [24] to transform time traces of photo-electron spectra into decay associated spectra.

4.5 Simulate Some Measurements

The results of equation (4.25) is shown in figure 4.2 with different time constants τ_2. The maximum of the population in state $|2\rangle$ shifts to to higher time delays if the state becomes more stable.

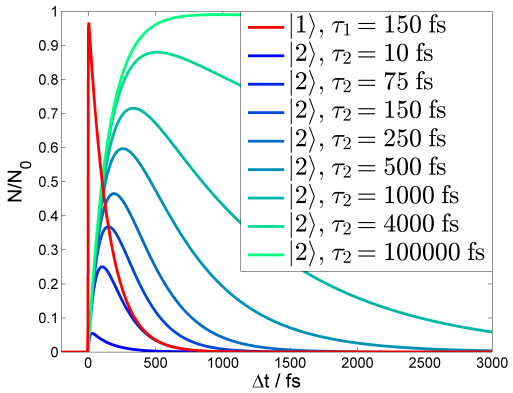

Figure 4.2: Simulated population of state $|1\rangle$ and $|2\rangle$ with the time constant $\tau_1 = 150\,\text{fs}$ and $\sigma = 50\,\text{fs}$. The population of state $|2\rangle$ is drawn with different time constants τ_2.

Figure 4.4 shows that it is impossible to get τ_2 if the population of state $|2\rangle$ is fitted with an exponential decay and $\tau_2 < \tau_1$. Only if $\tau_2 > \tau_1$ and the integration interval starts at about $10\tau_1$ it is possible to get the right τ_2 from the exponential fit. But with this condition state $|1\rangle$ is quasi empty (population left $\approx 4.5E^{-3}\%$). If $\tau_1 = \tau_2$ it is pretty much impossible to get the right τ_2. It is not possible to detect the mistake because the fit error is always very small.

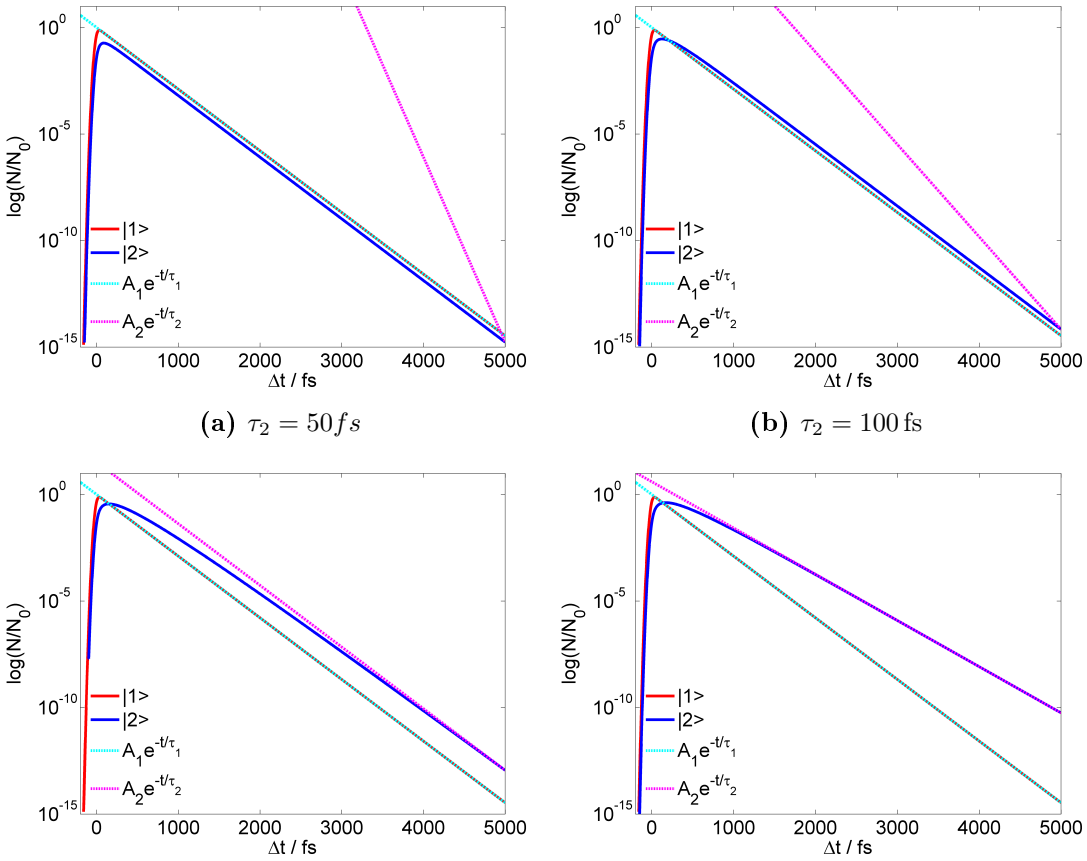

(a) $\tau_2 = 50fs$ **(b)** $\tau_2 = 100\,\text{fs}$

(c) $\tau_2 = \tau_1 = 150\,\text{fs}$ **(d)** $\tau_2 = 200\,\text{fs}$

Figure 4.3: In figure (a) - (d) $\tau_1 = 150\,\text{fs}$ and $\sigma = 50\,\text{fs}$. A clear trend is visible: If $\tau_1 > \tau_2$ ((a) and (b)) then the decay of state $|2\rangle$ is dominated by the time constant τ_1 (cyan curve; blue curve is parallel to cyan curve). If $\tau_1 < \tau_2$ (d) the population of state $|2\rangle$ decays exponentially with the time constant τ_2 (magenta curve - blue curve is parallel to magenta curve). If $\tau_1 = \tau_2$ the population of state $|2\rangle$ decays after a time delay Δt of about 4000 fs ($\approx 27\tau_1$) approximately exponentially with a time constant of τ_2. After a certain time delay Δt the population of state $|2\rangle$ will decay exponentially with the time constant τ_2 but this certain Δt becomes bigger if the difference of $\tau_1 - \tau_2$ gets bigger.

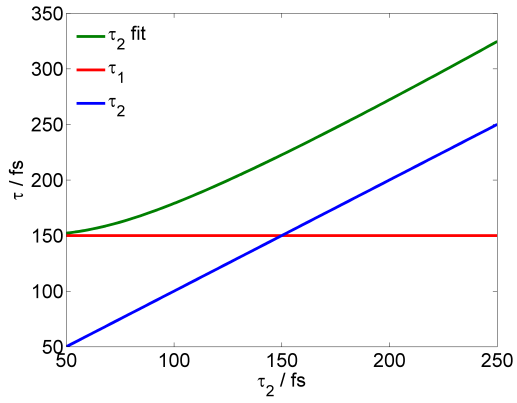

(a) Range of fit = 300 - 1200 fs

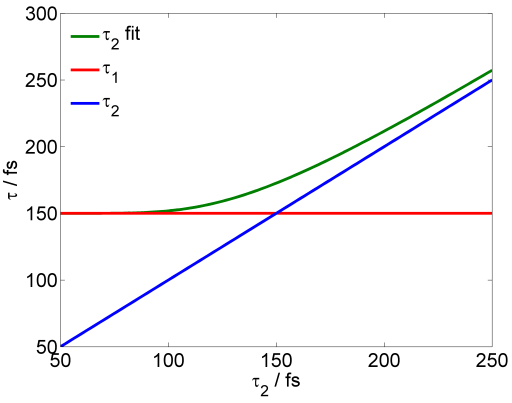

(b) Range of fit = 1000 - 2000 fs

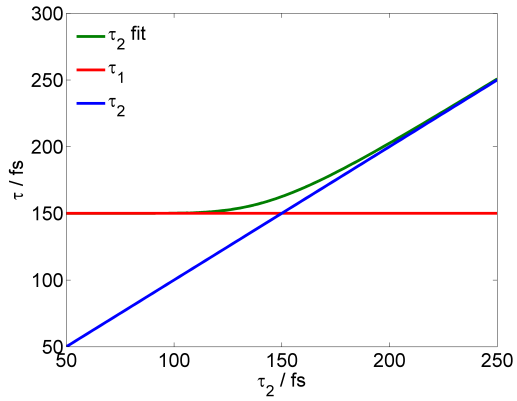

(c) Range of fit = 1800 - 5000 fs

Figure 4.4: In all simulations $\tau_1 = 150\,\text{fs}$ and $\sigma = 50\,\text{fs}$. A function $Ae^{-\frac{t}{\tau_2^{fit}}}$ was fitted on $N_2(t)$ (eq. (4.25)) with the data from a given time interval. The green curve is the fitted time constant τ_2^{fit}. The blue curve is the real τ_2 and the red curve is τ_1. σ is too small to have an influence on the fit result in the tested integration intervals. (a) - (c) show that fitting the temporal behaviour of the population of state $|2\rangle$ with an exponential decay gives only the right time constant τ_2 if it is bigger than τ_1 and when the integration interval starts about 10 times τ_1. This means that state $|1\rangle$ is only $4.5E^{-3}\%$ filled!

4.6 Time Constants of Acetone

The different dynamics of the molecule are discussed in much more detail in [11] and [8].

4.6.1 Spectra

Figure 4.5 shows the photo-electron spectrum at 50 fs and at 300 fs time delay. Peaks corresponding to different states and energy intervals are assigned in table 4.1. The parent signal shows a big peak around 2.5 eV which decays very fast. The spectrum of the fragment signal looks at the two time delays very similar. In [8] single pulse spectra were measured with the same photon energy (395 nm) as in this experiment. The spectra have the same edge at about 3.1 eV and a similar shape. The peak positions, and therefore the peak assignment in this measurement also agree very well with the spectra in [8]. The different photo-electron peaks are better visible in this measurement because the time delay between exciting the molecule and ionizing it is bigger and therefore more states are decayed.

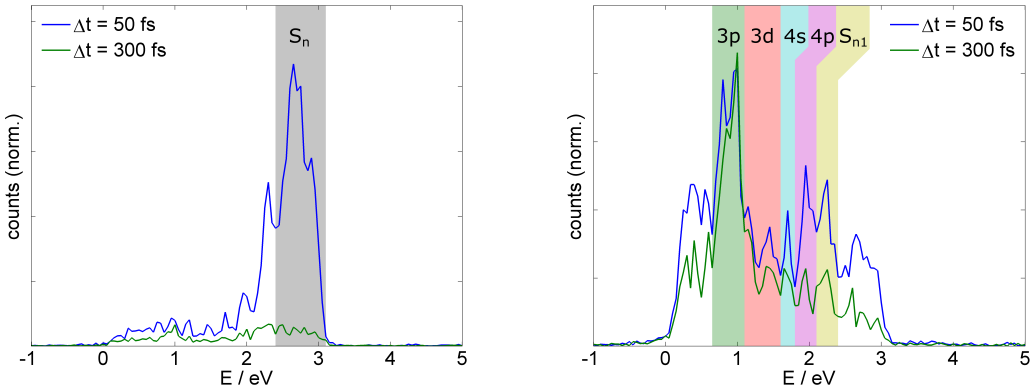

(a) Parent signal: near $\Delta t = 0$ fs a strong signal at about 2.5 eV is visible. This signal decays very fast.

(b) Fragment signal: the change in the fragment spectrum is minor. The form of the spectrum changes a bit.

Figure 4.5: Photo-electron spectrum of parent and fragment at 50 fs and 300 fs. The shaded areas label the different molecular states. The acetone molecule was excited with 3×395 nm (9.42 eV) and ionized with another 395 nm (3.14 eV). The ionisation potential of acetone is 9.7 eV [21] - without concerning the spectral width of the pulses a photo-electron signal up to about 2.86 eV energy is expected. With the spectral width the maximum photo-electron energy should be at 3.02 eV (spectral width ≈ 0.04 eV) which can be seen in (a) and (b).

Figure 4.6 shows the photo-electron spectra at different time delays. The parent signal has one big structure which decays rather fast. Other smaller peaks can be seen as well but they are overshadowed by the big structure at about 2.7 eV. The fragment spectra are much more interesting because there are multiple peaks visible. The peak at about 0.7 eV has a local minimum at about 0.15 ps which can be explained by the fit model introduced in 4.1 (with a small modification explained in section 4.6.2).

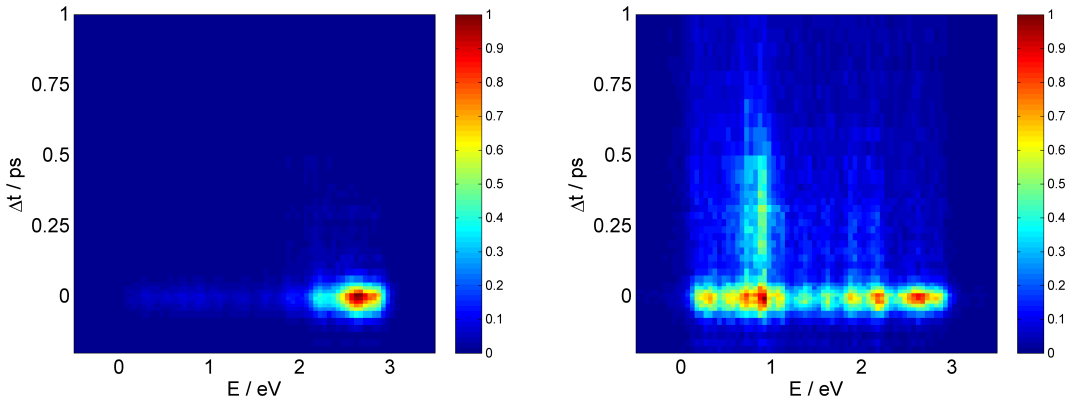

(a) Parent: A high signal can be seen at a small time delay. This signal decreases rather fast. At lower photo-electron energies small structures can be seen.

(b) Fragment: A lot of structures over the whole photo electron range can be seen. The signal at about 0.7 eV shows a local minimum at a time delay of about 0.15 ps followed by another maximum.

Figure 4.6: Spectra of parent and fragment over different time delays. Energy resolution: 0.05 eV.

4.6.2 Time constants of Acetone

At a small time delay the pump and the probe pulses start to overlap. The signal in the spectra is therefore described by the model derived in 4.1 and an added Gaussian function. The signal yield is proportional to the intensity of the pulses to the power of the number of photons needed for the ionisation process [7]. If the the intensity is changed this law is not directly observable because of saturation effects in the ionisation volume (the number of photons needed is underestimated and usually not an whole number). This additional channel can be described with a Gaussian.

In [11] the different relaxation dynamics of acetone were studied. There the high energy parent state at about 2.7 eV is directly populated (model state $|1\rangle$) and all other states are populated due to relaxation (model state $|2\rangle$). As described by the model the

Table 4.1: Overview of energy intervals and state assignment.

Molecule	Energy interval	State type	State
Fragment	0.65 eV - 1.1 eV	$\|2\rangle$	$3p$
Fragment	1.1 eV - 1.6 eV	$\|2\rangle$	$3d$
Fragment	1.6 eV - 1.8 eV	$\|2\rangle$	$4s$
Fragment	1.8 eV - 2.1 eV	$\|2\rangle$	$4p$
Fragment	2.1 eV - 2.4 eV	$\|2\rangle$	S_{n1}
Parent	2.4 eV - 3.1 eV	$\|1\rangle$	S_n

population of $|2\rangle$ is coupled with the population of state $|1\rangle$. Therefore, the transient population of $|1\rangle$ can be fitted with transient population of $|2\rangle$.

In order to fit the spectra different energy bands are integrated and then fitted (see table 4.1). The energybands correspond to different acetone states [8]:

Two different type of fits are used:

- Global fit: Fit all spectra at the same time. The advantage is that data from $|2\rangle$ contribute to the fit parameters of $|1\rangle$. This fit has stable results when started at different starting points.
- Sequential fit: First fit $|1\rangle$ and then fit $|2\rangle$ with the fit parameters of $|1\rangle$. This leads to highly unstable results because the fit parameters of $|1\rangle$ are fixed while fitting $|2\rangle$. This results depended on the starting point of the fits and therefore the results are not trustworthy.

Figure 4.7 shows the result of the fit. The fit model fits very well to the data. In the fragment spectrum the signal increase at a time delay of about 150 fs is explainable by the model. The time constants of the different states are listed in table 4.2.

σ of the Gaussian that fills the state and the added Gaussian are set equal (fit: $\sigma = (35.74 \pm 0.28)$ fs). The reason is that two σ act on the same part of the spectra (at about $\Delta t \approx 0$). Therefore, the different σ can not be disentangled. Also, the two σ are very similar because the σ for the filling of state $|1\rangle$ is a three photon process. The ionisation of the molecule is a four photon process. This means that the two Gaussian have approximately the same width.

Further interpretation is necessary but the results will lead two peer-reviewed journal publications: one describing the Bayesian probability subtraction and a second presenting

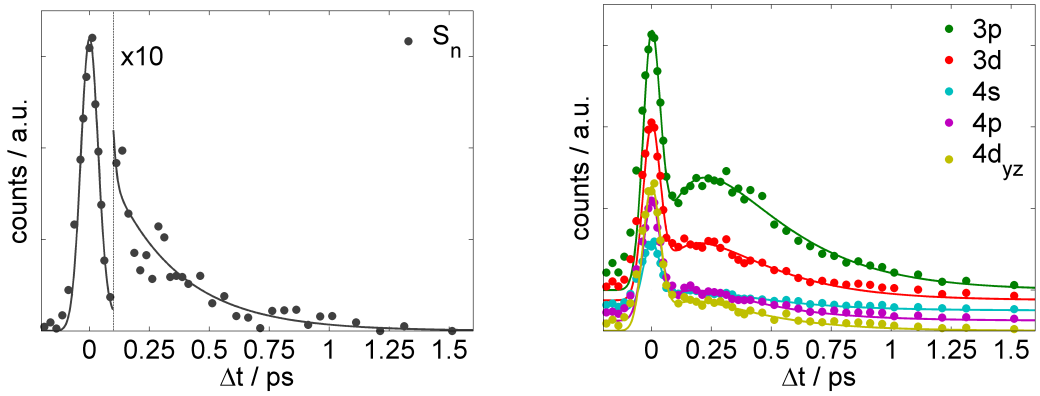

(a) Parent **(b)** Fragment

Figure 4.7: Fit result of the time scan. The model fits perfectly on the data. The rise in the fragment signal is well modelled.

Table 4.2: Time constants of the different parent and fragment states.

Molecule	State	τ / fs	$\Delta\tau$ / fs
Fragment	$3p$	175	20
Fragment	$3d$	138	21
Fragment	$4s$	134	51
Fragment	$4p$	114	29
Fragment	S_{n1}	110	27
Parent	S_n	284	25

the relaxation dynamics in acetone.

CHAPTER 5

Appendix

5.1 True to False Channel Ratio

It is possible to calculate the channel resolved true to false coincidence ratio for more than 2 states:

$$\begin{aligned} tf^i_{SC} = \frac{p_{true}}{p_{false}} &= \frac{p(1,1|\lambda_i,\xi_e,\xi_i)\prod_{j\neq i} p(0,0|\lambda_j,\xi_e,\xi_i)}{\sum_{j,k=0}^{N} p(1,0|\lambda_j,\xi_e,\xi_i)p(0,1|\lambda_k,\xi_e,\xi_i)} \\ &= \frac{\lambda_i\left(1+\lambda_i(1-\xi_e)(1-\xi_i)\right)}{2\sum_{k=1}^{N}\sum_{j>k}^{N}\lambda_k\lambda_j(1-\xi_e)(1-\xi_i)} \end{aligned} \tag{5.1}$$

5.2 Estimate Spectral Distribution

From a pump-probe spectrum and the pump-only spectrum it is not only possible to calculate the spectrum from the probe part of the pump-probe measurement but also the spectral distribution. The difference is that the probe spectrum has an absolute height (number of coincidences) and is zero in the time bin where no counts were detected. The spectral distribution is normalized and the estimation for the spectral distribution is never zero because it is not possible to be 100% sure that at a photo-electron will be never detected at a given flight time. Note that if in the coincidence spectrum a structure becomes smaller and another stays the same that in the spectral distribution its vice versa. To understand this it is important to understand what $q_{\beta 2\nu}$ is. $q_{\beta 2\nu}$ is the probability that if a photo-electron originates from the probe pulse it will be detected

at the time bin t_ν. If a structure shrinks and another stays the same the probability that a photo-electron originates from the probe pulse gets smaller. Also in the spectrum the probability that a photo-electron will be detected at the shrinking structure gets smaller - on the other hand the probability that a photo-electron that originates from the probe pulse is more likely to be detected in the structure that stays at the same height.

To calculate the spectral distribution the marginalization rule is used:

$$p(\mathbf{q}_{\beta 2}|\mathbf{n}_\alpha, \mathbf{n}_\beta, P_{\beta 1}) = \underbrace{\prod_{\nu=1}^{L} \sum_{n_{\beta 2\nu}=0}^{n_{\beta\nu}}}_{\sum_{\{\mathbf{n}_{\beta 2}\}}} p(\mathbf{q}_{\beta 2}|\mathbf{n}_\alpha, \mathbf{n}_\beta, P_{\beta 1}, \mathbf{n}_{\beta 2}) p(\mathbf{n}_{\beta 2}|\mathbf{n}_\alpha, \mathbf{n}_\beta, P_{\beta 1}) \tag{5.2}$$

The probability $p(\mathbf{n}_{\beta 2}|\mathbf{n}_\alpha, \mathbf{n}_\beta, P_{\beta 1})$ is given in equation (3.36) and was derived in section 3.5:

$$p(\mathbf{n}_{\beta 2}|\mathbf{n}_\alpha, \mathbf{n}_\beta, P_{\beta 1}, \mathbf{N}) \propto \frac{\kappa^{N_\beta - N_{\beta 2}}}{\Gamma\left(N_\alpha + N_\beta - N_{\beta 2} + C\right) N_{\beta 2}!} \prod_{\nu=1}^{L} \frac{\Gamma\left(n_{\alpha\nu} + n_{\beta\nu} - n_{\beta 2\nu} + c_\nu\right)}{(n_{\beta\nu} - n_{\beta 2\nu})!}$$

There was also $p(\mathbf{q}_{\beta 1}|\mathbf{n}_\alpha, \mathbf{n}_\beta, P_{\beta 1}, \mathbf{n}_{\beta 2})$ calculated. The calculation of $p(\mathbf{q}_{\beta 2}|\mathbf{n}_\alpha, \mathbf{n}_\beta, P_{\beta 1}, \mathbf{n}_{\beta 2})$ follows exactly the same strategy. Therefore, this distribution can be determined to:

$$p(\mathbf{q}_{\beta 2}|\mathbf{n}_\alpha, \mathbf{n}_\beta, P_{\beta 1}, \mathbf{n}_{\beta 2}) \propto N_{\beta 2}! \delta\left(\sum_{\nu=1}^{L} q_{\beta 2\nu} = 1\right) \prod_{\nu=1}^{L} \frac{q_{\beta 2\nu}^{n_{\beta 2\nu}+d_\nu-1}}{n_{\beta 2\nu}!} \tag{5.3}$$

Again a Dirichlet prior with the variable d_ν is used.
The result so far is:

$$\begin{aligned} p(\mathbf{q}_{\beta 2}|\mathbf{n}_\alpha, \mathbf{n}_\beta, P_{\beta 1}) = \frac{1}{Z} \sum_{\{\mathbf{n}_{\beta 2}\}} \frac{\kappa^{N_\beta - N_{\beta 2}}}{\Gamma\left(N_\alpha + N_\beta - N_{\beta 2} + C\right)} \delta\left(\sum_{\nu=1}^{L} q_{\beta 2\nu} = 1\right) \\ \prod_{\nu=1}^{L} \frac{q_{\beta 2\nu}^{n_{\beta 2\nu}+d_\nu-1}}{n_{\beta 2\nu}!} \frac{\Gamma\left(n_{\alpha\nu} + n_{\beta\nu} - n_{\beta 2\nu} + c_\nu\right)}{(n_{\beta\nu} - n_{\beta 2\nu})!} \end{aligned} \tag{5.4}$$

For the computation of the momenta $\langle q_{\beta 2\mu}^n \rangle$ equation (5.4) must be multiplied by $q_{\beta 2\mu}^n$ and then integrated over all $q_{\beta 2\mu}$. The result is the same as calculating the normalization constant Z and change the variable $d_\mu \to d_\mu + n$.

Therefore, it is useful to calculate Z. The integral is the norm of the Dirichlet distribution times some factors which does not depend on $\mathbf{q}_{\beta 2}$. This integral was also calculated in 3.5:

$$\begin{aligned} Z &= \int_0^1 \left(\prod_{\nu=1}^{L} dq_{\beta 2\nu} \right) p(\mathbf{q}_{\beta 2} | \mathbf{n}_\alpha, \mathbf{n}_\beta, P_{\beta 1}) \\ &= \sum_{\{\mathbf{n}_{\beta 2}\}} \frac{\kappa^{N_\beta - N_{\beta 2}}}{\Gamma(N_{\beta 2} + D)\,\Gamma(N_\alpha + N_\beta - N_{\beta 2} + C)} \\ &\prod_{\nu=1}^{L} \frac{\Gamma(n_{\beta 2\nu} + d_\nu)\,\Gamma(n_\alpha + n_{\beta\nu} - n_{\beta 2\nu} + c_\nu)}{(n_{\beta\nu} - n_{\beta 2\nu})! n_{\beta 2\nu}!} \\ &= \sum_{\{\mathbf{n}_{\beta 2}\}} Z_{n_{\beta 2}} \end{aligned} \tag{5.5}$$

Note that $\sum_{\nu=1}^{L} d_\nu = D$.

In order to calculate $\langle q_{\beta 2\mu} \rangle$ set $d_\mu \to d_\mu + 1$ and therefore $D \to D + 1$ and calculate Z'. The ratio of Z' and Z is the expectation value:

$$\begin{aligned} \langle q_{\beta 2\mu} \rangle = \frac{Z'}{Z} &= \frac{1}{Z} \sum_{\{\mathbf{n}_{\beta 2}\}} \frac{\kappa^{N_\beta - N_{\beta 2}}}{\Gamma(N_{\beta 2} + D + 1)\,\Gamma(N_\alpha + N_\beta - N_{\beta 2} + C)} \\ &\prod_{\nu \neq \mu} \frac{\Gamma(n_{\beta 2\nu} + d_\mu)\,\Gamma(n_\alpha + n_{\beta\nu} - n_{\beta 2\nu} + c_\mu)}{(n_{\beta\nu} - n_{\beta 2\nu})! n_{\beta 2\nu}!} \\ &\frac{\Gamma(n_{\beta 2\mu} + d_\mu + 1)\,\Gamma(n_\alpha + n_{\beta 2\mu} - n_{\beta 1\mu} + c_\mu)}{(n_{\beta\mu} - n_{\beta 2\mu})! n_{\beta 2\mu}!} \\ &= \sum_{\{\mathbf{n}_{\beta 2}\}} \frac{Z_{n_{\beta 2}}}{Z} \frac{n_{\beta 2\mu} + d_\mu}{N_{\beta 2} + D} \end{aligned} \tag{5.6}$$

The second moment can be calculated with the same strategy. Only change $d_\mu \to d_\mu + 2$:

$$\begin{aligned}\langle q^2_{\beta 2\mu}\rangle = \frac{1}{Z}\sum_{\{\mathbf{n}_{\beta 2}\}} & \frac{\kappa^{N_\beta - N_{\beta 2}}}{\Gamma\left(N_{\beta 2}+D+2\right)\Gamma\left(N_\alpha+N_\beta-N_{\beta 2}+C\right)} \\ & \prod_{\nu\neq\mu}\frac{\Gamma\left(n_{\beta 2\nu}+d_\mu\right)\Gamma\left(n_\alpha+n_{\beta\nu}-n_{\beta 2\nu}+c_\mu\right)}{(n_{\beta\nu}-n_{\beta 2\nu})!n_{\beta 2\nu}!} \\ & \frac{\Gamma\left(n_{\beta 2\mu}+d_\mu+2\right)\Gamma\left(n_\alpha+n_{\beta 2\mu}-n_{\beta 1\mu}+c_\mu\right)}{(n_{\beta\mu}-n_{\beta 2\mu})!n_{\beta 2\mu}!} \\ = \sum_{\{\mathbf{n}_{\beta 2}\}} & \frac{Z_{n_{\beta 2}}}{Z}\frac{(n_{\beta 2\mu}+d_\mu+1)(n_{\beta 2\mu}+d_\mu)}{(N_{\beta 2}+D+1)(N_{\beta 2}+D)}\end{aligned} \tag{5.7}$$

In both momenta the factor $p_{n_{\beta 2}} = \frac{Z_{n_{\beta 2}}}{Z}$ appears. This is the probability distribution that should be sampled.
Again a MCMC Metropolis Hastings algorithm can be deviated because again most of the therms cancel out if in only one time bin one count is changed (note that the value of Z is not needed at any time):

MARKOV CHAIN MONTE CARLO ALGORITHM

Change $n_{\beta 2\mu} \to n_{\beta 2\mu}+1$:

$$p^+ = \frac{Z^+_{n_{\beta 2'}}}{Z_{n_{\beta 2}}} = \kappa^{-1}\frac{(N_\alpha+N_\beta-N_{\beta 2}+C-1)(n_{\beta 2\mu}+d_\mu)(n_{\beta\mu}-n_{\beta 2\mu})}{(N_{\beta 2}+D)(n_{\alpha\mu}+n_{\beta\mu}-n_{\beta 2\mu}+c_\mu-1)(n_{\beta 2\mu}+1)} \tag{5.8}$$

Change $n_{\beta 2\mu} \to n_{\beta 2\mu}-1$:

$$p^- = \frac{Z^-_{n_{\beta 2'}}}{Z_{n_{\beta 2}}} = \kappa\frac{(N_{\beta 2}+D-1)(n_{\alpha\mu}+n_{\beta\mu}-n_{\beta 2\mu}+c_\mu)n_{\beta 2\mu}!}{(N_\alpha+N_\beta-N_{\beta 2}+C)(n_{\beta 2\mu}+d_\mu-1)(n_{\beta\mu}-n_{\beta 2\mu}+1)} \tag{5.9}$$

With $0 \leq n_{\beta 2\mu} \leq n_{n_{\beta\mu}}$

For $\langle q_{\beta 2\mu}\rangle$ sample $\frac{n_{\beta 2\mu}+d_\mu}{N_{\beta 2}+D}$
For $\langle q^2_{\beta 2\mu}\rangle$ sample $\frac{(n_{\beta 2\mu}+d_\mu+1)(n_{\beta 2\mu}+d_\mu)}{(N_{\beta 2}+D+1)(N_{\beta 2}+D)}$

If flat priors are used: $c_\nu = d_\nu = 1 \;\; \forall\nu \to C = D = L$.

5.3 Ideas for Improvement

5.3.1 Find Distribution for $N_{\beta 1}$ without Pre Estimating $P_{\beta 1}$

To calculate the probability $p(\mathbf{n}_{\beta 2}|\mathbf{n}_\alpha, \mathbf{n}_\beta, \mathbf{N}, P_{\beta 1})$ (eq. (3.29)) the approximation that $P_{\beta 1}$ is known was made. This approximation results in an underestimating of the variances because $p(N_{\beta 1}|\mathbf{N}, \mathbf{n})$ is broader than $p(N_{\beta 1}|\mathbf{N}, \mathbf{n}, P_{\beta 1})$. To avoid the approximation λ, ξ_e and ξ_i can be marginalized with the law of total probability and therefore $P_{\beta 1}$ can be calculated. To estimate λ, ξ_e and ξ_i three measured values are used like in section 3.10: The total number of coincidence counts N, the total number of detected electrons n_e and the total number of detected ions n_i. It would also be possible to take all coincidence values including for example the number of pulses where one ion and no electron is detected or three ions and two electrons. The idea would be the same but for the sake of readability the data from this coincidences are ignored. The abbreviations $\mathbf{N} = \begin{pmatrix} N_\alpha \\ N_\beta \end{pmatrix}$ and $\mathbf{n} = \begin{pmatrix} n_{e\alpha} \\ n_{i\alpha} \\ n_{e\beta} \\ n_{i\beta} \end{pmatrix}$ are used. To estimate the total number of coincidence counts that originates from the probe pulse the law of total probability is used to marginalize the mean number of ionization events for the pump-only measurement λ_α, the mean number of ionization events in the pump-probe measurement λ_β and the detection probabilities for electrons ξ_e and ions ξ_i:

$$\begin{aligned} p(N_{\beta 1}|\mathbf{N}, \mathbf{n}) = &\int_0^\infty d\lambda_\alpha \int_0^\infty d\lambda_\beta \int_0^1 d\xi_e \int_0^1 d\xi_i p(N_{\beta 1}|\mathbf{N}, \mathbf{n}, \lambda_\alpha, \lambda_\beta, \xi_e, \xi_i) \\ &\underbrace{p(\lambda_\beta, \xi_e, \xi_i|\mathbf{N}, \mathbf{n}, \lambda_\alpha)}_{=\Theta(\lambda_\alpha \leq \lambda_\beta) p(\lambda_\beta, \xi_e, \xi_i|\mathbf{N}, \mathbf{n})} p(\lambda_\alpha, \xi_e, \xi_i|\mathbf{N}, \mathbf{n}) \\ = &\int_0^\infty d\lambda_\alpha \int_{\lambda_\alpha}^\infty d\lambda_\beta \int_0^1 d\xi_e \int_0^1 d\xi_i p(N_{\beta 1}|\mathbf{N}, \mathbf{n}, \lambda_\alpha, \lambda_\beta, \xi_e, \xi_i) \\ &p(\lambda_\beta, \xi_e, \xi_i|\mathbf{N}, \mathbf{n}) p(\lambda_\alpha, \xi_e, \xi_i|\mathbf{N}, \mathbf{n}) \end{aligned} \tag{5.10}$$

The first probability distribution is a binomial distribution:

$$p(N_{\beta 1}|N_\alpha, N_\beta, \lambda_\alpha, \lambda_\beta, \xi_e, \xi_i) = \binom{N_\beta}{N_{\beta 1}} P_{\beta 1}^{N_{\beta 1}} \left(1 - P_{\beta 1}\right)^{N_\beta - N_{\beta 2}} \tag{5.11}$$

$$P_{\beta 1} = \frac{\lambda_\alpha(1 + \lambda_\alpha(1-\xi_e)(1-\xi_i))}{\lambda_\beta(1 + \lambda_\beta(1-\xi_e)(1-\xi_i))} \tag{5.12}$$

The third distribution can be evaluated with Bayes' theorem:

$$p(\lambda_\alpha, \xi_e, \xi_i|\mathbf{N}, \mathbf{n}, \xi_e, \xi_i) \propto p(N_\alpha|\mathbf{n}, \lambda_1, \xi_e, \xi_i)p(n_{e\alpha}|n_{i\alpha}, \lambda_1, \xi_e, \xi_i)p(n_{i\alpha}|\lambda_1, \xi_e, \xi_i)\cancel{p(\lambda, \xi_e, \xi_i)} \tag{5.13}$$

The distributions are the same as in section 3.10:

$$p(N_\alpha|\mathbf{n}, \lambda_\alpha, \xi_e, \xi_i) = \binom{N_p}{N_\alpha} p_{coin}^{N_\alpha}(1 - p_{coin})^{N_p - N_\alpha} \tag{5.14}$$

$$p_{coin} = \lambda_\alpha \xi_e \xi_i (1 + \lambda_\alpha(1-\xi_e)(1-\xi_i))e^{-\lambda_\alpha(1-(1-\xi_e)(1-\xi_i)} \tag{5.15}$$

$$p(n_{e\alpha}|n_{i\alpha}, \lambda_1, \xi_e, \xi_i) = \frac{(\lambda_\alpha N_p \xi_e)^{n_{e\alpha}}}{n_{e\alpha}!} e^{-\lambda_\alpha N_p \xi_e} \tag{5.16}$$

$$p(n_{i\alpha}|\lambda_\alpha, \xi_e, \xi_i) = \frac{(\lambda_\alpha N_p \xi_i)^{n_{i\alpha}}}{n_{i\alpha}!} e^{-\lambda_\alpha N_p \xi_i} \tag{5.17}$$

For $p(\lambda_\beta, \xi_e, \xi_i|\mathbf{N}, \mathbf{n}, \xi_e, \xi_i)$ the deviation looks exactly the same only the index α has to be replaced by β.
Because N_α, N_β and N_p are much greater than one, the binomial distribution can be approximated with a Gaussian:

$$\binom{N}{k} p^k (1-p)^{N-k} \approx \frac{1}{\sqrt{2\pi N p(1-p)}} e^{-\frac{(k-Np)^2}{2Np(1-p)}} \tag{5.18}$$

Also, the Poisson distributions can be approximated with a Gaussian because $\lambda N_p \xi$ and n are much larger than one:

$$\frac{\lambda^n}{n!} e^{-n} \approx \frac{1}{\sqrt{2\pi\lambda}} e^{-\frac{(n-\lambda)^2}{2\lambda}} \tag{5.19}$$

It should be possible to sample the probability distribution $p(\lambda_\beta, \xi_e, \xi_i|\mathbf{N}, \mathbf{n})p(\lambda_\alpha, \xi_e, \xi_i|\mathbf{N}, \mathbf{n})$ and then solve the integral in equation (5.10) with Monte Carlo integration.
If the result is compared with the estimation in section 3.10 it is clear that the estimation there is a maximum likelihood approximation.

5.3.2 Probability Distribution for False Coincidences

It would also be possible to take the probability into account that a parent coincidence count is in reality a fragment coincidence count. This would influence all the calculations so far where the spectra are separated before the evaluation. However, because the measurements are performed at low count rates and a high true to false coincidence ratio the probability to detect a fragment ion with an parent electron is very low and therefore neglectable.

List of Figures

List of Tables

Bibliography

[1] Markus Bainschab. Multiphoton Ionization Channels in Molecules Investigated by Photoelectron-Photoion-Coincidence Spectroscopy. Master's thesis, TU Graz, 2016.

[2] Andras Bodi, Tomas Baer, Nancy K Wells, Daniel Fakhoury, David Klecyngier, and James P Kercher. Controlling tunnelling in methane loss from acetone ions by deuteration. *Physical Chemistry Chemical Physics*, 17(43):28505–28509, 2015.

[3] Eric W-G Diau, Carsten Kötting, Theis I Sølling, and Ahmed H Zewail. Femtochemistry of Norrish Type-I Reactions: III. Highly Excited Ketones—Theoretical. *ChemPhysChem*, 3(1):57–78, 2002.

[4] HG Evertz. Computer Simulations. *URL: http://itp. tugraz. at/˜ evertz/Computersimulationen/cs. html*, 2009.

[5] Yehuda Haas. Photochemical α-cleavage of ketones: revisiting acetone. *Photochemical & Photobiological Sciences*, 3(1):6–16, 2004.

[6] IV Hertel and W Radloff. Ultrafast dynamics in isolated molecules and molecular clusters. *Reports on Progress in Physics*, 69(6):1897, 2006.

[7] T Ikuta, K Hosaka, H Akagi, A Yokoyama, K Yamanouchi, Fumihiko Kannari, and R Itakura. Separation of ionization and subsequent electronic excitation for formation of electronically excited ethanol cation in intense laser fields. *Journal of Physics B: Atomic, Molecular and Optical Physics*, 44(19):191002, 2011.

[8] Markus Koch, Pascal Heim, Bernhard Thaler, Markus Kitzler, and Wolfgang Ernst. Direct observation of a photochemical activation energy: A case study of acetone photodissociation. *Journal of Physics B: Atomic, Molecular and Optical Physics*, 2017.

[9] P Kruit and FH Read. Magnetic field paralleliser for 2π electron-spectrometer and electron-image magnifier. *Journal of Physics E: Scientific Instruments*, 16(4):313, 1983.

[10] Paul Maierhofer. Femtosecond Photodissociation Dynamics in Molecules studied by Time-Resolved Phtoelectron-Photoion-Coincidence Spectroscopy. Master's thesis, TU Graz, 2016.

[11] Paul Maierhofer, Markus Bainschab, Bernhard Thaler, Pascal Heim, Wolfgang E Ernst, and Markus Koch. Disentangling Multichannel Photodissociation Dynamics in Acetone by Time-Resolved Photoelectron–Photoion Coincidence Spectroscopy. *The Journal of Physical Chemistry A*, 120(32):6418–6423, 2016.

[12] Akitaka Matsuda, Mizuho Fushitani, Chien-Ming Tseng, Yasumasa Hikosaka, John HD Eland, and Akiyoshi Hishikawa. A magnetic-bottle multi-electron-ion coincidence spectrometer. *Review of Scientific Instruments*, 82(10):103105, 2011.

[13] Waike Moos. *Stochastische versus deterministische Trends im Rahmen der Cointegration: Bayesianische Simulationsstudien.* Springer-Verlag, 2013.

[14] Nerijus Rusteika, Klaus B Møller, and Theis I Sølling. New insights on the photodynamics of acetone excited with 253- 288nm femtosecond pulses. *Chemical Physics Letters*, 461(4):193–197, 2008.

[15] Péter Sándor, Vincent Tagliamonti, Arthur Zhao, Tamás Rozgonyi, Matthias Ruckenbauer, Philipp Marquetand, and Thomas Weinacht. Strong field molecular ionization in the impulsive limit: Freezing vibrations with short pulses. *Physical review letters*, 116(6):063002, 2016.

[16] Aparna Shastri and Param Jeet Singh. Vibrational modes in excited Rydberg states of acetone: A computational study. *Journal of Quantitative Spectroscopy and Radiative Transfer*, 173:92–105, 2016.

[17] Theis I Sølling, Eric W-G Diau, Carsten Kötting, Steven De Feyter, and Ahmed H Zewail. Femtochemistry of Norrish Type-I Reactions: IV. Highly Excited Ketones—Experimental. *ChemPhysChem*, 3(1):79–97, 2002.

[18] Albert Stolow, Arthur E Bragg, and Daniel M Neumark. Femtosecond time-resolved photoelectron spectroscopy. *Chemical reviews*, 104(4):1719–1758, 2004.

[19] Vincent Tagliamonti, Péter Sándor, Arthur Zhao, Tamás Rozgonyi, Philipp Marquetand, and Thomas Weinacht. Nonadiabatic dynamics and multiphoton resonances in strong-field molecular ionization with few-cycle laser pulses. *Physical Review A*, 93(5):051401, 2016.

[20] Bernhard Thaler. Ultrafast molecular photodissociation dynamics studied with single-pulse femtosecond photoelectron-photoion-coincidence spectroscopy. Master's thesis, TU Graz, 2017.

[21] Wayne M Trott, Normand C Blais, and Edward A Walters. Molecular beam photoionization study of acetone and acetone-d 6. *The Journal of Chemical Physics*, 69(7):3150–3158, 1978.

[22] Wolfgang von der Linden, Volker Dose, and Udo Von Toussaint. *Bayesian probability theory: applications in the physical sciences*. Cambridge University Press, 2014.

[23] Iain Wilkinson, Andrey E Boguslavskiy, Jochen Mikosch, Julien B Bertrand, Hans Jakob Wörner, David M Villeneuve, Michael Spanner, Serguei Patchkovskii, and Albert Stolow. Excited state dynamics in SO2. I. Bound state relaxation studied by time-resolved photoelectron-photoion coincidence spectroscopy. *The Journal of chemical physics*, 140(20):204301, 2014.

[24] Guorong Wu, Andrey E Boguslavskiy, Oliver Schalk, Michael S Schuurman, and Albert Stolow. Ultrafast non-adiabatic dynamics of methyl substituted ethylenes: The π 3s Rydberg state. *The Journal of chemical physics*, 135(16):164309, 2011.

Danksagung

Bedanken möchte ich mich als erstes bei meinem Betreuer Ass.Prof. Dipl.-Ing. Dr. techn. Markus Koch für das sehr angenehme Betreuungsverhältnis. Ich hatte während der gesamten Arbeit immer das Gefühl auf Augenhöhe mit ihm zu arbeiten. Jede meiner Fragen wurde gewissenhaft beantwortet und meine Meinung wurde immer sehr geschätzt. Er lies mich schnell selbstständig arbeiten und hatte viel Vertrauen in meine Fähigkeiten. Das er immer mit offenen Karten spielt und Probleme schnell und direkt anspricht sorgt für ein gutes Zusammenarbeiten.

Mein nächster Dank gilt meinem Laborpartner Bernhard Thaler mit dem ich unzählige Stunden im fensterlosen Labor verbracht habe, das manchmal lediglich mit Laserlicht erhellt wurde. Die Zusammenarbeit mit ihm war immer sehr harmonisch, unkompliziert und wir hatten stets viel Spaß. Dadurch verging auch jede noch so langwierige justagearbeit sehr schnell.
An dieser Stelle möchte ich noch meinen Dank an unsere Nachfolger Sascha Ranftl und Stefan Cesnik zum ausdruck bringen.
Für die Möglichkeit am Institut für Experimentalphysik meine Masterarbeit zu schreiben möchte ich Herrn Univ.-Prof. Dr. Wolfgang E. Ernst danken.

Paul Maierhofer und Markus Bainschab möchte ich für den tollen Start in die Masterarbeit danken. Dank ihrer sehr guten Einschulung wurde die Arbeit mit dem komplexen Aufbau erst möglich. Es war sehr faszinierend für mich wie gut und schnell sie viel von ihrem know-how ans uns weitergegeben haben.

Für die vielen interesannten und schönen Kaffeepausen und dem wöchentlichen Toasty Tuesday / Noodle Wednesday möchte ich Martin Schnedlitz, Max Lasserus, Roman Messner, Alexander Schiffmann und Florian Lackner hiermit Danke sagen.

Einen großen Dank gilt Michael Rumetshofer und Univ.-Prof. Wolfang von der Linden für die Zusammenarbeit beim entwickeln des Bayes' Algorithmus.

Einen weiteren großen Dank gilt meinen Freunden aus Graz, welche das Studien und Freizeitleben erheblich versüßten. Dazu zählen unter anderem Nina Schneider, Tobias Achtsnit, Robert Stindl, Julian Pilz, Martin Tazreiter, Georg Greil, Fabian Muralter, Markus Gößler, Christoph Winkler und viele andere.

Dank gilt auch meinen Freunden aus Vorarlberg dessen Bindung zu ihnen die große Distanz und teilweise langen Abwesenheiten nichts anhaben kann. Dieses unkomplizierte und enge Verhältnis lässt jeden Besuch in der Heimat sich so anfühlen, als ob man nie weg gewesen wäre.

Zu guter letzt möchte ich mich noch bei meinem Vater Franz und meiner Schwester Claudia bedanken für die tolle Unterstützung in den letzten Jahren und das ermöglichen dieses Studiums.